REPORT DOCUMENTATION PAGE

AFRL-SR-BL-TR-99-

0033

1. AGENCY USE ONLY (Leave blank)	2. REPORT DATE	3. REPOR
	January 1999	Fina

4. TITLE AND SUBTITLE

The Interaction of Kinetic Energy Penetrators with Geomaterials and Concrete

5. FUNDING NUMBERS

F49620-98-1-0090

6. AUTHOR(S)

C. A. Ross
M. J. Schmidt
N. D. Cristescu
O. Cazacu

7. PERFORMING ORGANIZATION NAME(S) AND ADDRESS(ES)

University of Florida
UFGERC
1350 N. Poquito Road
Shalimar, FL 32579

University of Florida
UFAEMES
P. O. Box 116250
Gainesville, FL 32611-6250

8. PERFORMING ORGANIZATION REPORT NUMBER

9. SPONSORING/MONITORING AGENCY NAME(S) AND ADDRESS(ES)

Air Force Office of Scientific Research
Aerospace & Materials Sciences
AFOSR/NA
110 Duncan Ave., Suite B115
Bolling AFB, DC 20332-0001

10. SPONSORING/MONITORING AGENCY REPORT NUMBER

11. SUPPLEMENTARY NOTES

12a. DISTRIBUTION/AVAILABILITY STATEMENT

Approved for public release
Distribution unlimited

12b. DISTRIBUTION CODE

13. ABSTRACT (Maximum 200 words)

A large diameter split Hopkinson pressure bar (SHPB) was used to generate dynamic shear strength and confined/unconfined compressive data for mortar. In addition quasistatic shear and compressive strength data were generated for the same mortar. The new shear specimen was modeled using finite element analysis to verify its validity. Strain rate sensitivity of the shear response of mortar is very similar to that of the tension and compression data. A new elastic/viscoplastic constitutive equation was developed for mortar. This equation, rather simple in concept and expression, captures the main features of the material response such as compressibility and dilatancy strain-hardening, influence of the loading rate and creep and relaxation. This model can be easily extended to 3-D conditions.

14. SUBJECT TERMS

Mortar, Dynamic Response, Shear Compression, Dilantacy, Elastic Viscoplastic, Static Response

15. NUMBER OF PAGES

16. PRICE CODE

17. SECURITY CLASSIFICATION OF REPORT	18. SECURITY CLASSIFICATION OF THIS PAGE	19. SECURITY CLASSIFICATION OF ABSTRACT	20. LIMITATION OF ABSTRACT
unclassified	unclassified	unclassified	UL

The Interaction of Kinetic Energy Penetrators With Geomaterials and Concrete

FINAL REPORT

C. A. Ross
M. J. Schmidt
University of Florida
Graduate and Engineering Research Center
1350 N. Poquito Road
Shalimar, FL 32579

N. D. Cristescu
O. Cazacu
University of Florida
Department of Aerospace Engineering, Mechanics
and Engineering Science
Post Office Box 116250
Gainesville, FL 32611-6250

U. S. Air Force Office of Scientific Research
Grant No. F49620-98-1-0090

PREFACE

This program was managed by the two co-principal investigators, Dr. C. A. Ross, University of Florida Graduate Engineering and Research Center (UFGERC), and Dr. N. D. Cristescu, University of Florida Department of Aerospace Engineering, Mechanics and Engineering Science (UFAEMES) under AFOSR contract F49620-98-1-0090, for the period December 1997 – November 1998. The program was originally scheduled for three years but the last two years were cancelled. Therefore, only a portion of the original proposal could be accomplished. The original program manager was Capt. M. Chipley and the current program manager is Dr. S. Walker of AFOSR/NA.

The shear response work of Section II was conducted by Mr. Martin Schmidt, graduate student of UFGERC, and he is the author of that section. The experimental data of Section III was obtained by Dr. C. A. Ross of UFGERC and he is the author of that section. Drs. N. D. Cristescu and O. Cazacu of UFAEMES developed the elastic/viscoplastic constitutive equation and are the authors of Section IV.

TABLE OF CONTENTS

LIST OF FIGURES

Figure

LIST OF TABLES

Table

SECTION I

EXECUTIVE SUMMARY

1. Objective

The major objectives of this study was to obtain quasistatic and dynamic experimental data relative to the effects of confining pressure on cementitious material and use that data to obtain required parameters for the development of a proposed elastic/viscoplastic constitutive model for concrete and geomaterials. A secondary objective was to select an experimental shear specimen and generate dynamic shear strength of concrete or mortar as a function of strain rate.

2. Background

Most materials have some sort of strain rate sensitivity giving increases in uniaxial material properties as the strain rate increases. Considerable data are available that show the effects of strain rate on strength properties of concrete when subjected to uniaxial tensile and compressive experimental tests. However, concrete and geomaterials such as rock and granite are pressure sensitive and effects of increased hydrostatic pressure is to increase the yield stress and strength, especially in compression. Some quasistatic triaxial data are available but very little dynamic triaxial data are available.

It is well known that even under reasonably high confining pressures concrete and rock show compressibility followed by cracking, swelling and dilatancy. Standard triaxial cells are necessary to produce quasistatic confining tests to generate low strain rate stress–strain behavior and volumetric changes of concrete and geomaterials. These tests are essential in the basic formulation of any constitutive modeling. In addition, dynamic triaxial stress-strain are also necessary to extend the range of constitutive modeling to include combined strain rate and confining pressure effects on basic compressive responses. Also, for a complete constitutive model

both tensile and shear response must be considered. The split Hopkinson pressure bar (SHPB) has been used extensively to obtain uniaxial compressive and tensile strengths of concrete and mortar and should lend itself to experimental testing in confined compression and unconfined shear response of these materials.

3. Scope

The general approach in this study is to use the SHPB to generate dynamic confined compressive and dynamic unconfined shear data for use in the development of a new elastic/viscoplastic model as a tool in the prediction of kinetic energy penetration into concrete and geomaterials. Additionally, quasistatic triaxial data will be obtained as the foundation for the model development.

4. Methodology

Concrete and mortar specimens obtained from outside sources were instrumented using electrical resistance strain gages. Some specimens were to be tested quasistatically in triaxial cells, some were tested unconfined quasistatically and the remainder were to be tested dynamically in both confined and unconfined modes in the SHPB. Strain and strain rate data were to be recorded directly from the instrumented specimens. Both longitudinal and transverse strains as well as the calculated volumetric strain are presented as functions of the principal stress difference. Shear response strength data will be obtained and shown in comparison to uniaxial compressive and tensile data as function of strain rate.

The experimental data as described above will be used in generating the necessary parameters to be inserted into the constitutive model. Application of the model will be limited and further modification will be continued in future studies.

It is necessary to note here that the original study was for three years. About half through the first year the last two years were cancelled causing a real problem trying to get something finished for a report. Also, the quasistatic triaxial cell data for concrete was contracted to an external source and these tests were delayed, only beginning at the writing of this report. For this reason the concrete data was not available for inclusion into the constitutive model and are not included in this report.

5. Results

Both confined and unconfined mortar tests were performed using a confining pressure cell mounted on a standard 3" Diameter (7.62cm) SHPB. Quasistatic compressive data was also conducted to determine unconfined compressive strength, Young's modulus and general compressive stress-strain behavior. For the unconfined mortar tests it is quite evident that the general stress-strain response is similar for quasistatic and dynamic tests however the strain rate effect is to produce increased strength at the high strain rates. Dynamic loading and strain rate tests were conducted at rates on the order of one hundred million times faster than the quasistatic tests. At these strain rates the compressive strengths are approximately double that of the quasistatic compressive test. The shear strengths at the higher strain rates was found to be as high as five times that of the quasistatic shear strength.

The confined dynamic tests showed similar stress-strain response as the quasistatic tests, even showing dilatancy at the higher principal stress differences. Effects of confining pressure on the compressive behavior is to increase the strength above that of the unconfined strength (at the same strain rate) but that increase occurs at a different stress-strain slope, giving an appearance of a work hardening phenomenon in concrete and mortar. It is interesting to note that the strain rate

observed by the SHPB signals for both confined and unconfined tests, for the same incident stress, are the same within experimental error.

A rate dependant constitutive model for mortar has been developed. The model reproduces strain hardening, load rate effects, creep and relaxation, observed compressibility and dilatancy.

SECTION II

DYNAMIC SHEAR RESPONSE OF MORTAR

1. Introduction

One of the primary damage mechanisms related to blast and impact loading on structures is shear failure. While there is a great deal of evidence to suggest that concrete is strain rate sensitive to tensile and compressive loads, little work is available regarding the rate sensitivity of concrete in shear. In order to investigate this phenomena, a suitable test specimen is required which is suitable for introduction into quasistatic and dynamic test apparatus. One possible design is presented and discussed here. It consists of a modified splitting tensile or "Brazilian" specimen in which two parallel notches are cut into the specimen to provide a shear plane. Quasistatic data is presented and compared to a finite element analysis of the proposed geometry. Finally, the specimen was introduced for testing into a Split Hopkinson Pressure Bar (SHPB). Results are presented which indicate a strong rate dependence of shear strength on strain rate.

The notion of shear failure in concrete is not without controversy. Many investigators in fact believe that failure in concrete is strictly a tensile phenomena. Yet in practice, structural elements loaded by an intense short-duration blast often fail by means of an apparent direct shear, characterized by the rapid propagation of a crack through the element's depth at the point of support [1]. It has also been reported by Heuze [2] that at velocities up to a few hundred meters per second, geologic material penetration is most dependent on target shear strength. Both phenomena are highly dynamic events in which the target material is subjected to high strain rates on the order of 10^1-10^4/sec. Concrete and other geomaterials have been reported by Ross et.al. [3] and Malvern et.al. [4] to exhibit significant strength enhancement in both compression and tension at high loading rates. It is reasonable to assume that this same rate phenomena will be present in shear

behavior, however there is very little data available to quantify the effect. Murtha and Crawford [5] have reported that "due to the dearth of dynamic shear test data, the only apparent avenue for development of dynamic failure criteria is in terms of the static criteria modified by dynamic enhancement factors." The Air Force's Effectiveness/Vulnerability Assessments in Three Dimensions (EVA3D) [6] methodology for conventional weapon effects against structures makes use of such an empirical expression based on target geometry, the unconfined static strength of the concrete and a user defined constant.

1. Test Specimen and Quasistatic Tests

In order to develop improved models, one must first properly characterize the shear behavior of concrete. The first step in any such process would be the identification of a suitable specimen for testing. Richard [7] suggests that the essential requirements of a new shear test specimen include a simple compact geometry, ease of preparation, simple loading system, pure shear at the crack tip, and pure shear loading over large areas of the undisturbed specimen. For the purposes of this study, the additional constraint that it be easily implemented into a dynamic testing device such as the Split Hopkinson Pressure Bar (SHPB) [8] was also imposed. The specimen recommended by Richard for meeting his criteria, while well suited for metals, would not be easily fabricated with geomaterials. It would also prove difficult to implement into a SHPB. Bazant and Pfeiffer [9] has successfully performed direct shear tests on small, notched, four-point-loaded beam elements. This configuration, however, does not lend itself readily to implementation into the SHPB. Iosipescu [10] analyzed a number of potential geometries for shear testing making use of photoelastic stress analysis techniques. Once again, the sample ultimately recommended by Iosipescu would prove difficult to manufacture and implement into the SHPB. Barr [11, 12] has also reported on several candidate compact shear test specimens. The specimens were based on

either cubicle sections or cylinders, a form readily obtainable for concrete. Barr reported the best results for a cylindrically based model. The specimen, as depicted in Figure 1 is essentially a modified splitting tensile or "Brazilian" test . The modification, consisting of cutting two opposite parallel notches into the sample, was also relatively simple to perform. The shear strength of the material was evaluated from the load at failure as:

$$\tau = \frac{P}{dL}, \tag{1}$$

where, τ = the shear strength, P = the load at crack initiation, d = the notch separation distance, and L = the specimen length. Quasistatic test results using this sample were shown to be reproducible and relatively insensitive to the notch separation distance. Care had to be taken however in properly aligning the specimen in the load frame or shear failure was not observed. This specimen also has the advantage in that it can be readily implemented into the SHPB for dynamic testing. Figure 2 shows a schematic of the SHPB and the positioning of the compression, splitting tensile and shear specimen. Further discussion of the principle of operation of the SHPB is given in the next subsection. No modifications to the test apparatus is required for completion of the test. Based on the results of Barr and the suitability of the specimen for dynamic testing, the decision was made to proceed with testing of the cylindrical notched specimens.

A number of samples were cast for the study by the Air Base Technology Branch of the Air Force Research Laboratory's Materials Directorate at Tyndall A.F.B., FL. The material utilized was an aggregateless mortar of nominally 36.5 MPa compressive strength and 5.2 MPa tensile strength. The samples were cast in 76.2 mm diameter by 152.4 mm length molds, demolded at 24 hours and cured in water for 28 days. Upon removal from the water, they were cut into 38.1 mm lengths so that four samples could be fabricated from each mold. Notches were cut using a notch separation distance of 19 mm. The notch separation distance was chosen such that the specimens

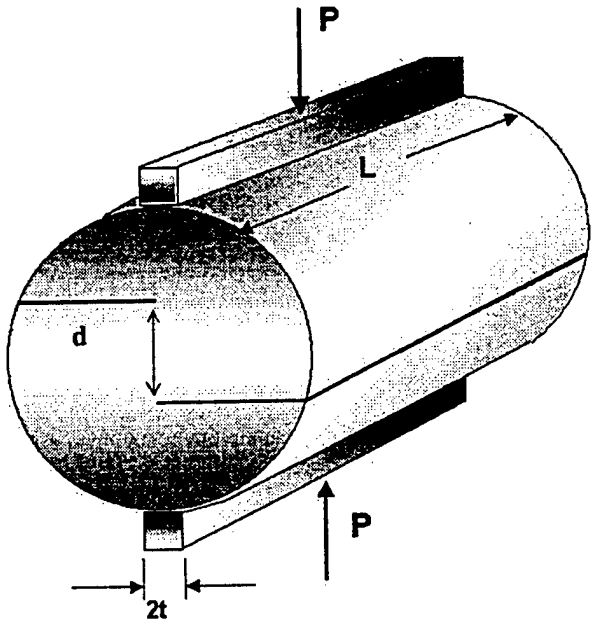

Figure 1. Proposed shear test specimen.

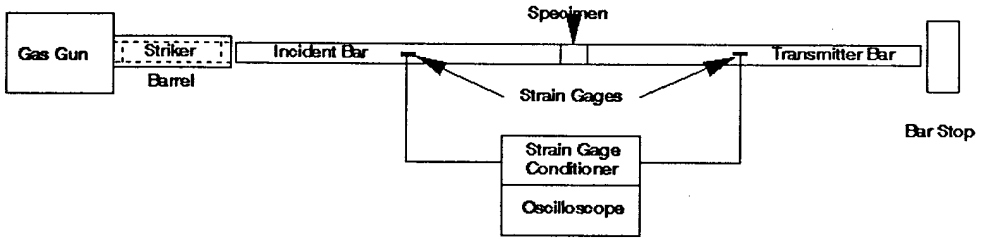

a) Split Hopkinson Pressure Bar (SHPB)

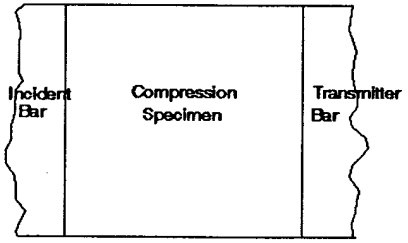

b) Specimen Arrangement for Compression Test

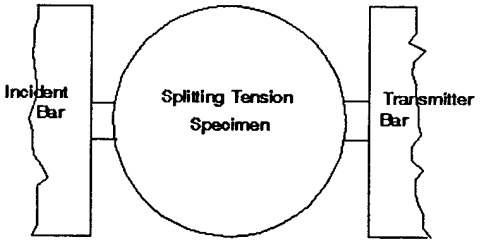

c) Specimen Arrangement for Splitting Tension Test

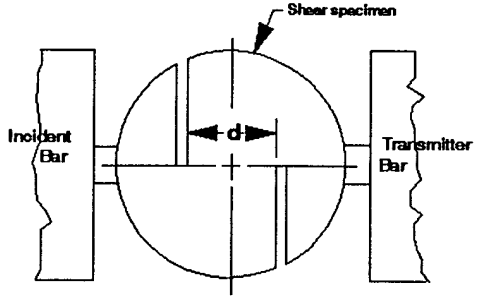

d)Specimen arrangement for shear test

Figure 2. Schematic of a split Hopkinson pressure bar (SHPB) showing an arrangement for the compressive, splitting tensile and shear specimens.

would be geometrically proportionate with those reported by Barr [11,12]. Tests were first performed quasistatically in an Instron 1332 servo-controlled load frame. Due to the similarity of the proposed shear test with the splitting tension test, the decision was made to conduct the tests at a constant load rate as called for in ASTM C 496-96. A total of three quasistatic tests were conducted. Results proved to be quite consistent with an average load at crack initiation of 4200 N (944 lbs). Figure 3 depicts a typical loading rate plot for a quasistatic test. The initial non-linearity can be attributed to setting of the loading strips. Specimen failure was indicated by the onset of a crack beginning at the root of one of the notches an propagating across the shear plane defined by the notch separation distance and the specimen length. Figure 4 depicts a typical quasistatic specimen failure.

3. Analysis

Based on the promising results of the quasistatic tests, the decision was made to conduct a finite element analysis on the geometry in order to gain better insight regarding the stress distribution in the sample. Since only the stress distribution was of interest, the material was modeled as an elastic, isotropic solid. No attempt was made to predict specimen failure. Elastic material parameters typical of concrete were chosen for use in the calculation. The calculations were carried out using ADINA [13]. The problem geometry and mesh were setup as depicted in Figure 5.

The load was modeled as a simple point source. While, it was recognized that this would result in unreasonably high stress concentrations in the areas directly adjacent to the load application, it is believed that these effects are highly localized and will not effect the results in the region of interest, that being in the vicinity of the notches and the plane they define. The average load at failure, as determined in the quasistatic tests, was selected as the applied load for the

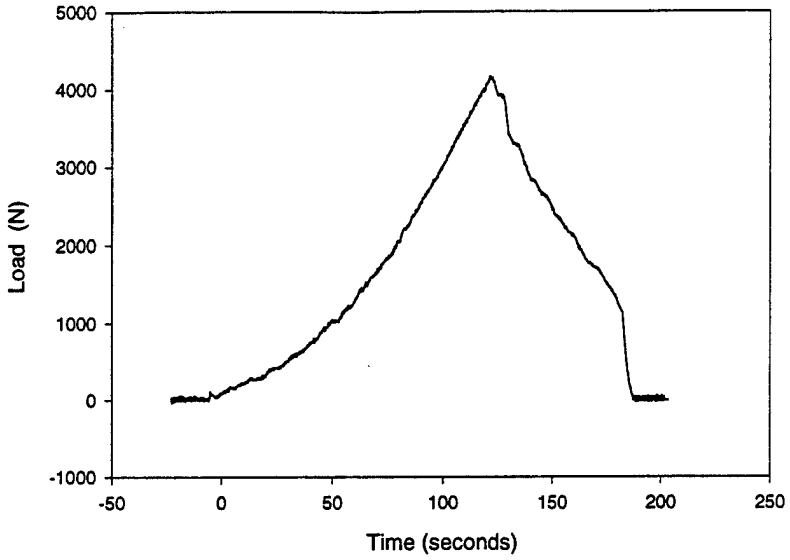

Figure 3. Load-time curve for a mortar quasistatic shear test.

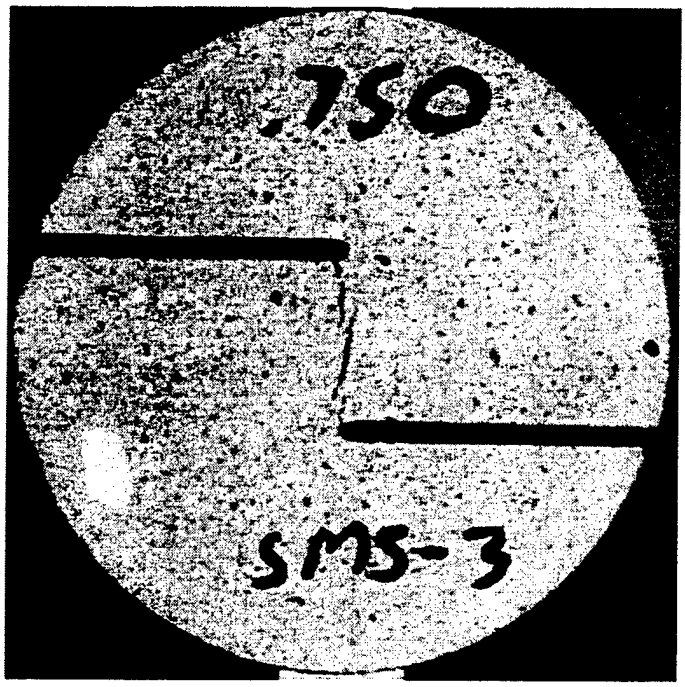

Figure 4. Failure mode of mortar quasistatic shear specimen.

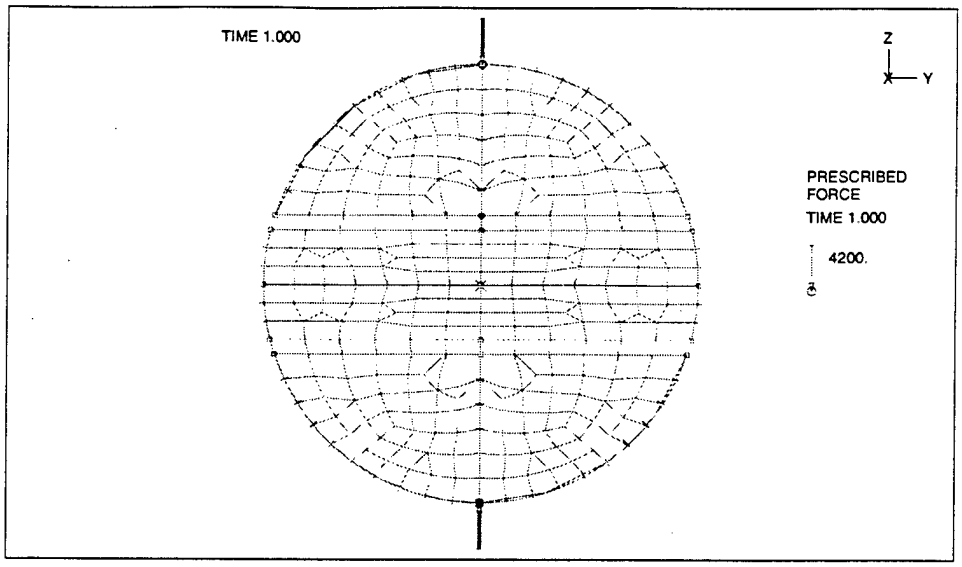

Figure 5. Finite element mesh used in the calculation.

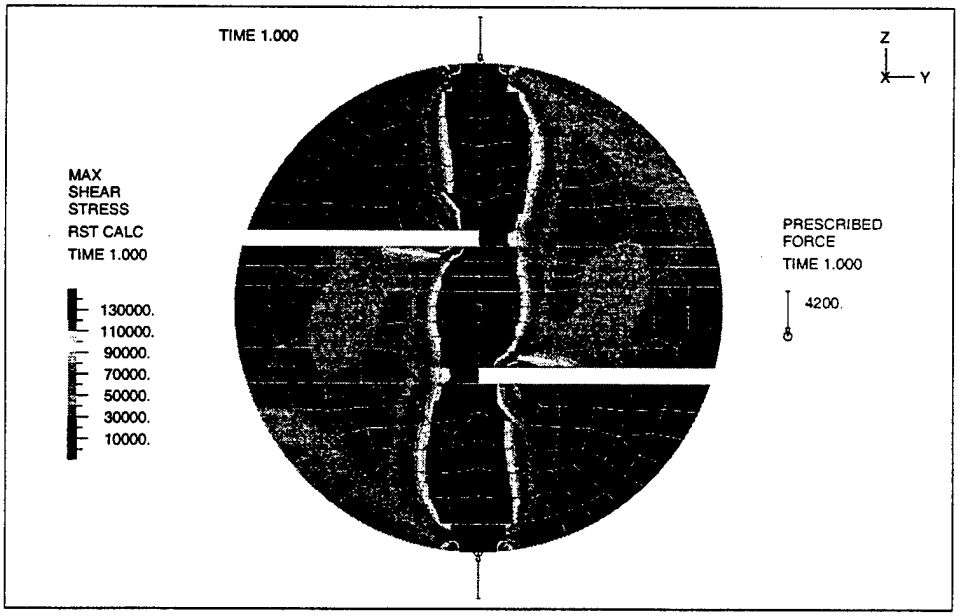

Figure 6. Band plot of stress distribution in shear specimen using the finite element method.

calculations. It was believed this would yield results indicative of the stress distribution near specimen failure. A band plot depicting the distribution of shearing stresses in the specimen is given in Figure 6. As can be seen, there is a zone of high shearing stresses along the plane defined by the two notches. Figure 7 is a plot showing the shearing load as well as the tension/compression loads along the line defined by the load application points. This plot has been overlaid with the specimen geometry in order to make visualization of the geometry effects easier. In the plots, tension is defined as positive and compression negative. Similar results have been obtained by Iosipescu [10] using photoelastic methods.

As predicted, there are very high tensile loads in the vicinity of the load application points. While artificially high as discussed above, they are indicative of localized crushing which likely occurs as the loading strips set. These loads are seen to diminish rapidly away from the application points, transitioning to high compressive loads at the notch tips. These loads are still well below the compressive strength of the material. In the area between the notches, there is a relatively uniform tensile zone of approximately 2 MPa. Once again, these tensile loads are significantly below the expected tensile failure stress. The shearing stresses are relatively low near the load application points and only become significant near the notch tips. The shear stresses can be seen to be fairly uniform between the notch tips and of significantly greater magnitude than the tensile loads. The mean shear load between the notches is approximately 4.8 MPa with a peak value at the inside edge of the notch of approximately 6.0 MPa. The calculated shear failure stress using Equation (1) and a peak load at cracking of 4200 N is approximately 5.8 MPa. Since the elastic properties entered into the material model were only approximate values typical of concrete in general, it is difficult to make any conclusive statements regarding the similarity of the experimental and analytical results. Yet, it is clear that the maximum calculated shearing stress

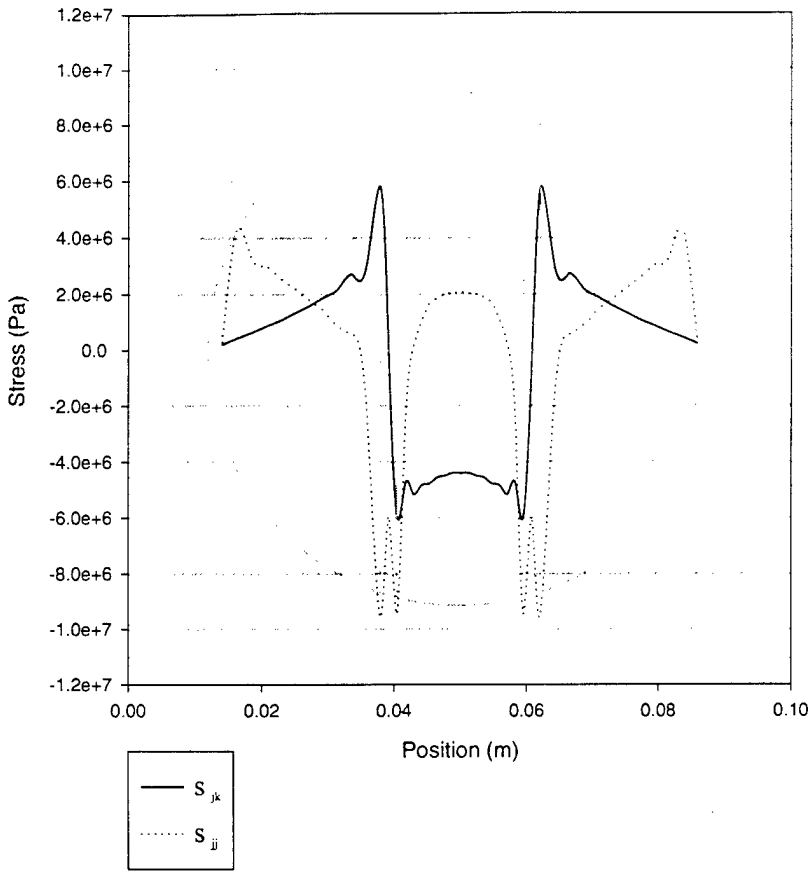

Figure 7. Calculated stress distribution in shear specimen using the finite element method.

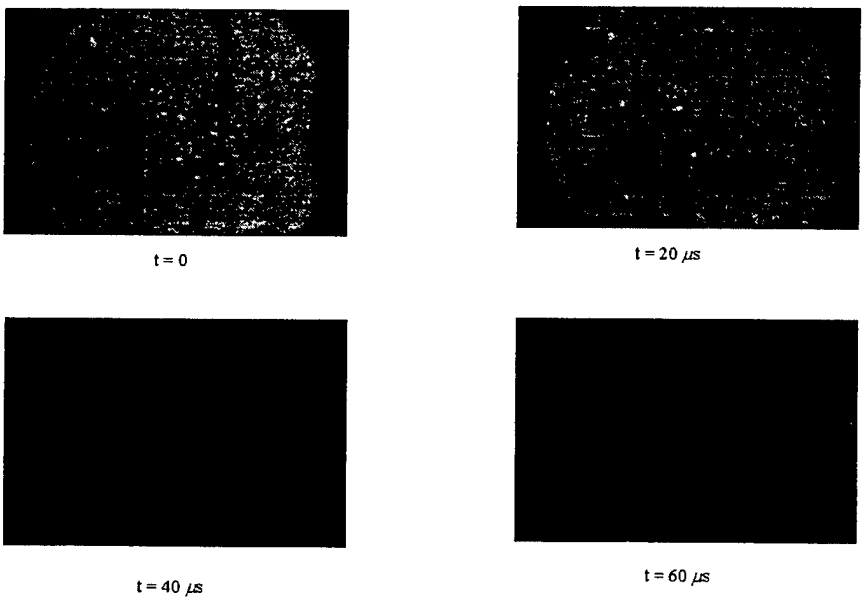

Figure 8. High speed photography of shear failure under dynamic loading.

closely approximates the measured value. Overall, the stress field is quite complex in the specimen and does not satisfy the requirements of Richard [7] that pure shear exist at the crack tip. There is however a highly concentrated shear zone between the notches, and according to Bazant and Pfeiffer [9], shear fracture propagation can exist provided such a concentrated shear zone exists. Therefore it is reasonable to conclude that the peak load recorded is in fact the maximum shearing load.

4. Dynamic Shear Tests

The next step in this study was to introduce the compact shear specimen into a SHPB for dynamic experimental analysis. The 76.2mm diameter SHPB located at the University of Florida's Graduate Engineering Research Center was utilized. The SHPB, shown schematically in Figure 2 produces a stress wave in the incident bar by impact of a striker bar. This stress wave impinges on the specimen and is partially reflected into the incident bar and partially transmitted into the transmitter bar. The stress in the specimen is proportional to the magnitude of the transmitted pulse and the strain rate in the specimen is proportional to the slope of the load curve. Use of the SHPB in high strain rate testing is well documented in the literature by Ross[8] and Follansbee [14]. In order to verify that the specimen was failing due to shear induced cracking between the notches, an Imacon high-speed digital imaging camera was utilized to record crack initiation and propagation. The Imacon is capable of recording at frame rates up to one million per second. Unfortunately, it is only capable of obtaining eight frames of information. A frame rate of 20 microseconds between frames was found to be adequate to capture crack initiation and provide a few frames of propagation. A total of seven high strain rate tests were conducted. Figure 8 shows the digital imaging for one of these tests. The crack is just visible at 20 microseconds and has propagated nearly completely across the gap between the notches by 40 microseconds.

Dynamic shear strength was calculated from the expression:

$$\tau_d = \frac{P_d}{dL}, \qquad (2)$$

where τ is the dynamic shear strength and P_d is the dynamic load, taken from the peak of the transmitted stress pulse as measured in the SHPB transmitter bar. The dynamic shear terms were then normalized by dividing through by the quasistatic strength. This normalized value is referred to as a Dynamic Increase Factor, or DIF. This was then plotted along side normalized tension and compression data as a function of strain rate. The results are depicted in Figure 9.

As can be seen, the shear data lies intermediate between the tensile and compression data with a slope similar to the tensile data. There appears to relatively little scatter in the data, with all the points very nearly falling on a linear fit drawn through the data. The shear strength appears to be highly rate sensitive, with values of DIF of nearly 5 recorded at a strain rate of approximately 20/sec. This is in the general area of interest for conventional explosive effects.

5. Discussion

The compact double notched cylindrical shear test specimen, originally proposed by Barr was analyzed and found to be well suited for both quasistatic and dynamic analysis of concrete shear strength. The stress distribution within the specimen was found to be quite complex, though a zone of concentrated shear loading did exist between the two notch tips. Quasistatic and dynamic tests were conducted. Results were quite consistent in both cases. The dynamic shear strength of concrete was found to be quite rate sensitive with values somewhat intermediate between the compression and tension data. It is quite obvious that for calculations regarding the response of structures under highly dynamic loads, simply using empirical formulas based on quasistatic data is not adequate. An expression based on the dynamic shear strength or tensile strength would be more appropriate. Further testing is recommended to evaluate notch separation distance sensitivity.

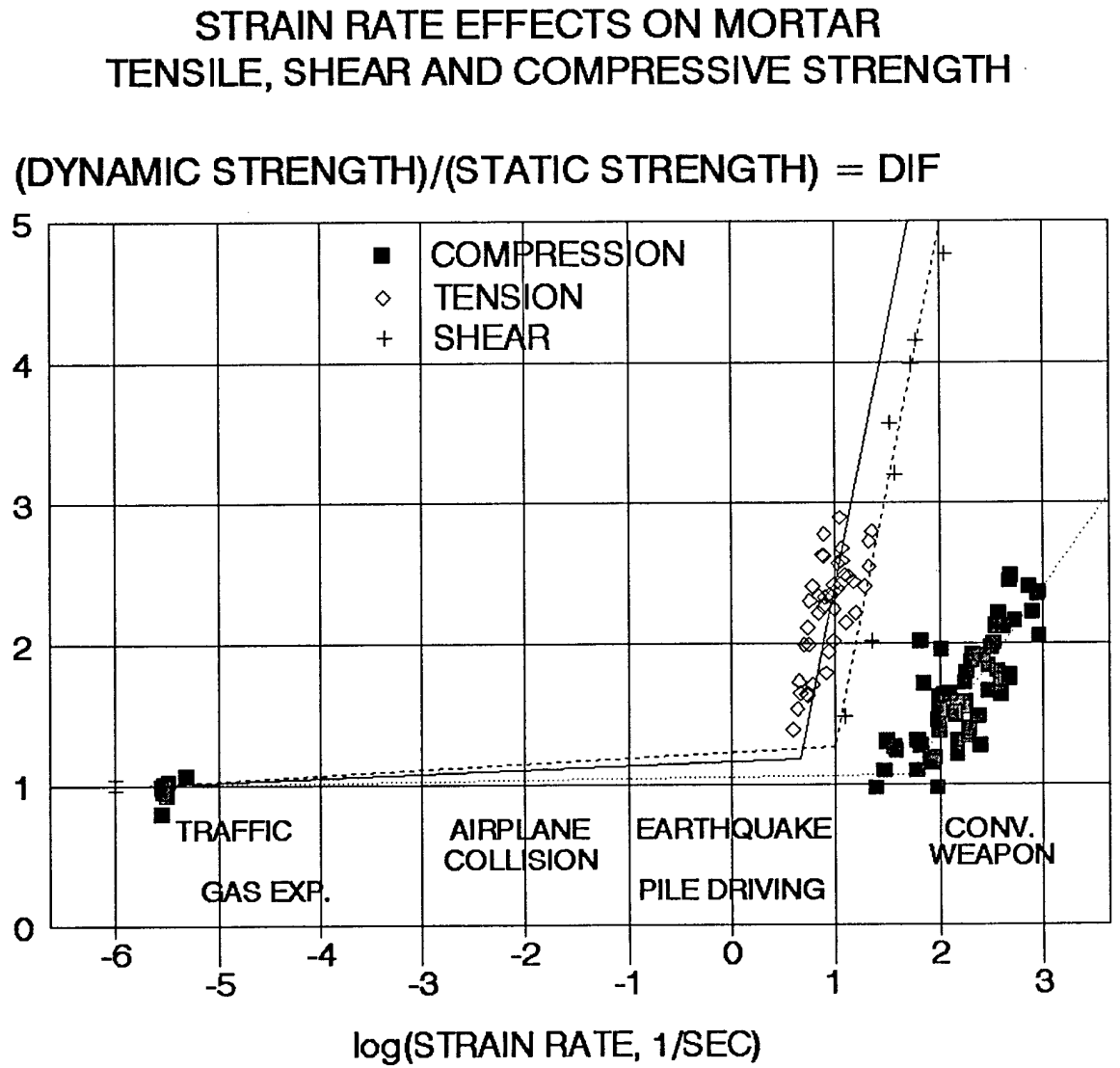

Figure 9. General strain rate effects on mortar strength.

Tests on concrete with representative size aggregate must also be conducted. Finally, a detailed dynamic finite element analysis should be conducted to evaluate the state of stress near failure under dynamic conditions.

Section III

CONFINED AND UNCONFINED MORTAR TESTS

1. Introduction

In an effort to produce experimental data for use in determining parameters of the basic constitutive equation given later in Section IV, a series of experiments were conducted using specimens of a mortar mix. The proportions for this mix are given in Table 1 and the 28 day quasistatic properties are given in Table 2.

Table 1
Mix Proportions for Mortar

Portland Cement	450g
Sand, Sieve #4	1620g
WRDA-19 0.5%	3.7g
"F" Fly Ash	297g
Water, w/c = 0.55	411g

Table 2
28 Day Quasistatic Properties Of Concrete
(4" Diameter x 8" Long Specimen)

Compressive Strength, $f_c' = 6120$ PSI (42.2 MPa)
(Approximate Strain Rate 6.7×10^{-6}/sec)
Tensile Strength (Sp. Ten.) 430 PSI (3.0 MPa)
(Approximate Strain Rate 3.76×10^{-7}/sec)
Density w =130 lbs/ft^3 (2080 kg/m^3)
Comp. Modulus, $33\, w^{3/2}\sqrt{f_c'} = 3.83 \times 10^6$ PSI (26.4 GPa)

Due to the long time between casting date and time of testing the mortar compressive strength was measured using the same 3" Diameter x 3" Long (76.2mm x 76.2mm) specimens as used for the dynamic confined and unconfined tests. The compressive strength at the approximate time of the dynamic tests was 7220 PSI (49.8 MPa) and the calculated modulus was 4.16×10^6 PSI

(28.7 GPa). The average modulus determined by the unconfined quasistatic compression test using electrical resistance strain gages on the specimen was 3.62 x 10^6 PSI (25.0 GPa).

2. Split Hopkinson Pressure Bar and Confining Cell

A. Split Hopkinson Pressure Bar (SHPB)

The SHPB used for the dynamic confined and unconfined mortar tests is a 3" diameter (76.2mm) device located at the University of Florida Graduate and Engineering Center (UFGERC) in Shalimar, Florida. This device is powered by compressed nitrogen gas driving a 30" long (0.762m) striker bar of the same diameter as the incident and transmitter bars. A schematic of the SHPB is shown in Figure 2. In the compressive mode of operation the striker bar impacts the incident bar and imparts a compressive stress pulse in the incident bar. This stress pulse impinges on the specimen, sandwiched between the incident and transmitter bars. Due to the impedance mismatch between the specimen material and the bar material and or the cross sectional area differences, the stress pulse is partially reflected back into the incident bar and partially transmitted into the transmitter bar. It can be shown [8] that the stress in the specimen is proportional to the transmitted pulse and the strain and strain rate are proportional to the reflected pulse. For the SHPB tests of this study the transmitter bar strain signals were used to determine the axial stress of the specimen. The strain rate of the test was determined using the reflected signal. Since, electrical resistance strain gages were mounted directly on the specimen, the specimen strains were determined using these strain signals. The strain rate measured by the SHPB reflected strain signals agreed very well with the strain rate measured using the specimen strains. Detailed discussion of the acquisition of the strain signals from strain gages on the individual bars of the SHPB is omitted here for brevity and for additional information on this subject the reader is directed to References [8 and 14].

B. Confining Pressure Cell

The confining pressure cell used in this study is the same cell used by Malvern and Jenkins [15] in their study of the effects of strain rate and confinement on the compressive strength of concrete. A schematic of the cell is shown in Figure 10 with the specimen sandwiched between the bars of the SHPB. For this study the confining pressure acting transverse to the specimen was matched by an axial pressure on the bars. This was accomplished by using a fixed collar on the incident bar and exerting pressure using a hydraulic piston on the distal end of the transmitter bar away from the specimen. This configuration gives a hydrostatic pressure in the fully confined tests.

In the preparation for a test the various pieces of the confining cell were placed on the respective bars for assembly after test specimen placement. The instrumented specimen shown in Figure 11 is placed between the two bars and a slight axial pressure is applied to hold it in place. The epoxy coated strain gage leads are taped to the bar a distance far enough to clear the 'O' rings and allow for the positioning of the 'O' rings, compression rings and compression nuts. The epoxy coated strain gages leads from the specimen prevents the grounding of the leads to the bar. The very small diameter of the leads (gauge 34) allows for good seating of the 'O' rings to the membrane and bars.

Once the specimen is in place a layer of aluminum tape is placed over the specimen in an effort to prevent damage of the membrane by small voids of the specimen and any cracks at the bar-specimen interfaces. Once the specimen is sealed the rubber membrane is stretched over the specimen, the 'O' rings are lubricated and forced in place and held in place by the compression rings followed by tightening of the large compression nuts.

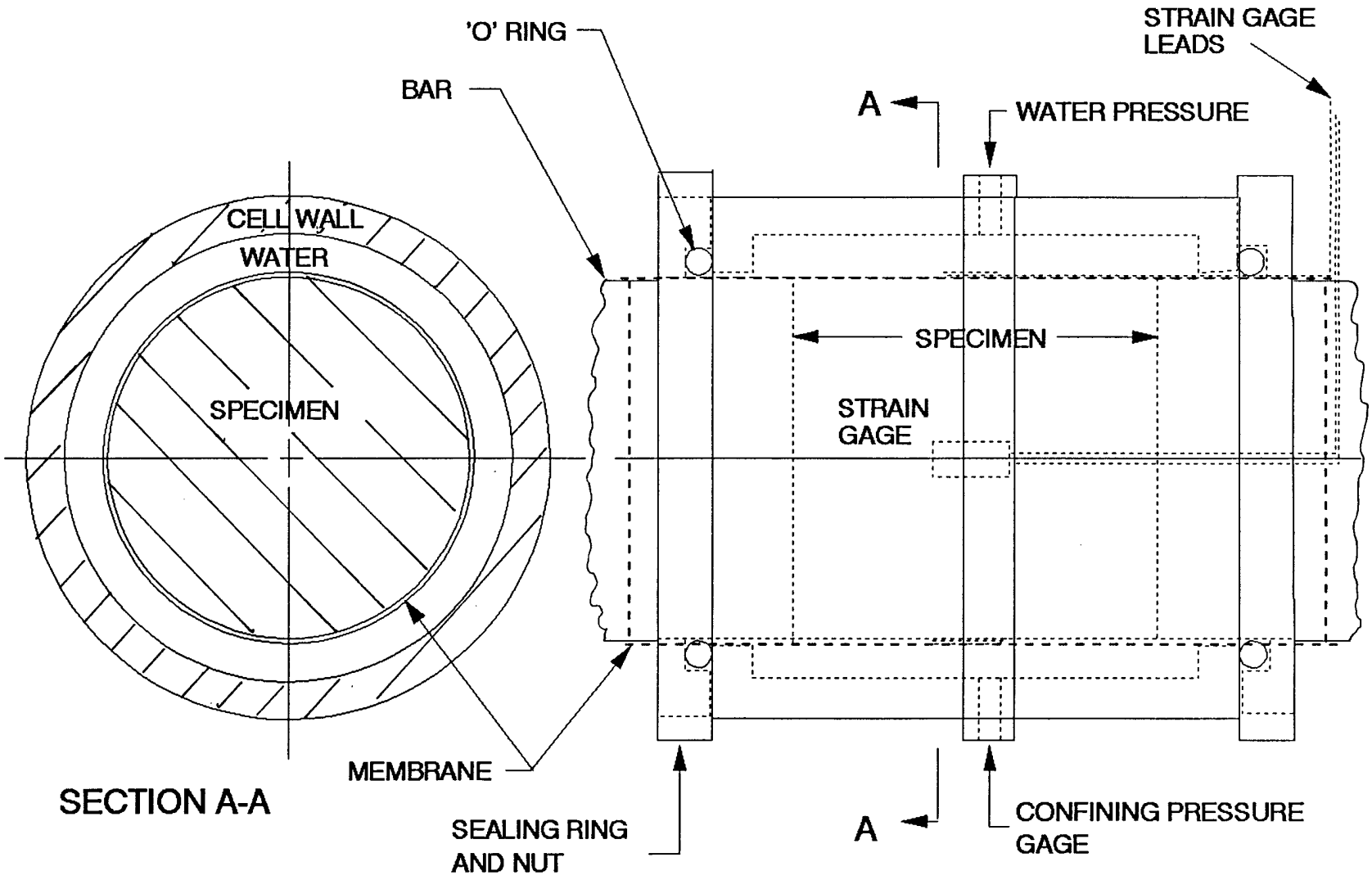

Figure 10. Schematic of confining pressure cell.

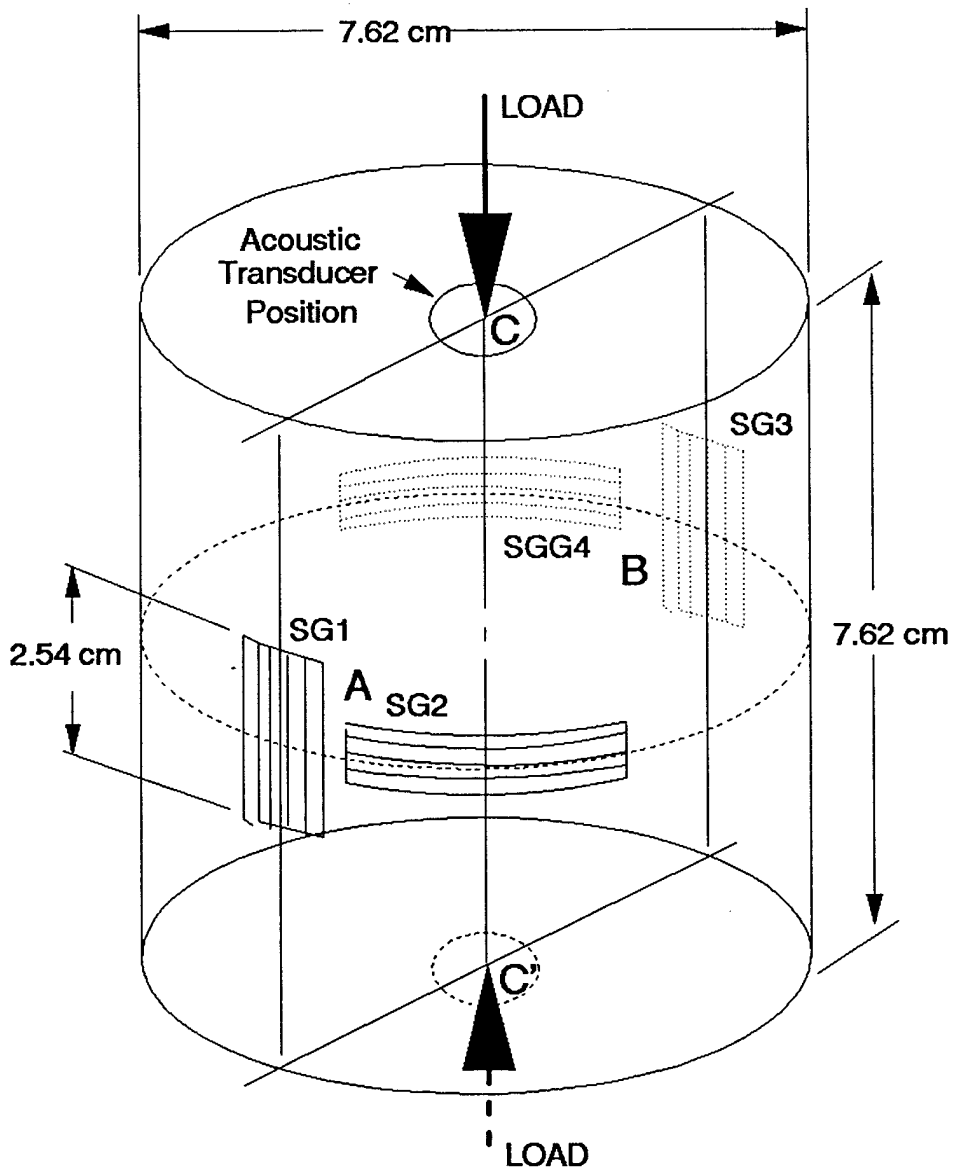

Figure 11. Schematic showing the strain gage locations on the test specimen.

3. Experiments

A. Specimen Instrumentation

For both quasistatic and dynamic tests a nominally 3" Diameter x 3" Long (7.62cm D x 7.62cm L) specimen was used. All test specimens were instrumented, by two pairs of a longitudinal and a transverse electric resistance strain gage, as shown in Figure 11. Each specimen was lightly sanded with 120 grit sandpaper and dust removed by application of acid and neutralizer solutions prescribed for strain application cleaning. Strain gage epoxy adhesive (Micromeasurements M-Bond AE-10) was applied to fill voids. The adhesive was allowed to dry 24 hours, sanded and cleaned again before application of the strain gages. The strain gages were manufactured by Micromeasurements and designated as EA-06-500BH-120. Both 1.0 inch (2.54cm) and 0.5 inch (1.27cm) gage lengths were used with a 120 ohm gage resistance. The specimen strain gages were connected in an external wheatstone bridge with a "dummy" temperature compensating gage mounted on a mortar specimen placed near the test area. Precision 120 ohm resistors were used as completion resistors in the circuit. The external bridge was connected to a 2311 Micromeasurements Strain Gage Conditioner and Amplifier which was connected to a 4094B Nicolet oscilloscope for the dynamic test and a PRO40 Nicolet oscilloscope for the quasistatic tests. All signals recorded by the oscilloscopes were subsequently transferred to computer disk for storage. The data was then converted to stresses and strains and read into ASCII files using a VUPOINT software package.

B. Quasistatic Tests

Quasistatic tests were conducted using an Instron 1332 servo-controlled load frame with loads and strains recorded using a Nicolet oscilloscope. The quasistatic tests were

conducted to determine the compressive strength and Young's modulus as well as the longitudinal and transverse strains from the specimen. All quasistatic tests were unconfined and run under a load-control mode. Details of the tests and data from these tests are given later in a Test Summary.

C. Dynamic Tests

Both confined and unconfined dynamic tests were conducted using the SHPB. For the unconfined tests the confining pressure cell was removed and the specimen was allowed to expand as in a normal SHPB strength test as described in Reference [8]. The exception in this case is that the strains on the specimen were recorded as described previously. For the unconfined and confined SHPB tests the strain signals from the incident and transmitter bars (Figure 2) were also recorded. The strain signals from incident bar strain gages, which includes the incident and reflected strain pulse, were used in the standard fashion for determining the incident stress and strain rate in the specimen. The strain signal of the transmitter bar strain gage was used in the standard fashion for determining the axial load or stress in the specimen. The standard SHPB assumption of uniformity of the stress along the specimen length was used here in determining the specimen stress.

For the confined SHPB tests two methods of establishing confining pressure were used. The first method consisted of simply filling the confining pressure cell with water and closing off all ports. A small amount of axial pressure was applied to the specimen as described previously. (This axial pressure is simply used to hold the specimen in place.) This method gives a zero initial confining pressure for the test. During the application of the impact stress pulse the confining pressure rises and is recorded using the pressure

transducer mounted in the confining pressure cell. The confining pressure is also recorded directly by the oscilloscope.

A second method of applying confining pressure to the specimen is by filling the confining cell with water and then pressurizing the water using a hand operated water pump. The confining pressure is monitored by a pressure gage on the hand pump and the recorded pressure by the pressure transducer. An axial stress of the same magnitude is applied to the SHPB simultaneously by a hydraulic jack and hand pump at the end of the transmitter bar away from the specimen. The axial stress is monitored using a pressure gage in series with the hydraulic pump and jack. During this test the pressure in the confining cell also rises and is recorded by the oscilloscope.

An alternate method of confining, also tried in this study, is to seal the confining cell with air trapped inside then pressurize the confining cell with the hand water pump and the simultaneous application of the axial stress. The general idea with this method is that the compressed air in the cell would tend to act as an accumulator and reduce the confining pressure rise. The confining pressure rise for this method was similar to the pressure rise of the second method described above.

After the specimen is mounted and the confining cell, if required, is put in place and the SHPB is operated in standard fashion. For this SHPB the loading pulse is 300 microseconds, but during the test the incident strain pulse is recorded approximately 280 microseconds ahead of the specimen strain gage pulses and the transmitted strain pulse is recorded approximately 280 microseconds after the beginning of the specimen strains. This means an oscilloscope recording time of at least 1200 microseconds is required. For these tests and in the standard SHPB test a recording time per point of 0.5 microsecond is used

which gives a recording window of approximately 1700 microseconds and allows for a trigger delay to observe any pre-trigger data that may occur.

For this study impact velocities, varied by the gas gun pressure, were adjusted to give three strain rates of approximately 60/sec, 120/sec and 160/sec. Due to inconsistencies in specimen strength and striker impact velocities the strain rates are not reproduced exactly with same gas gun pressure.

For these dynamic tests two four channel oscilloscopes were used to record the seven strain pulses. Since the specimen strain signals and other SHPB signals are not recorded at the same time a method of justifying the relative starting times of the signals was applied. It was assumed the longitudinal strain pulse of the specimen and the axial stress should be coincident in time, so the starting times of these two signals and the starting time of the confining pressure signal were adjusted to zero. Due to the Poisson effect the transverse specimen strain gage will not register as quickly as the longitudinal gage, so the transverse gage starting time was adjusted to zero at the same starting time of the longitudinal strain pulse.

D. Quasistatic and Dynamic Test Summary

The following kinds of tests were performed on 3" Diameter X 3" Long (7.62cm x 7.62cm) mortar specimens.

1. Quasistatic unconfined stress – strain test.
2. Quasistatic unconfined loading, unloading and reloading for modulus determination.
3. Dynamic unconfined at two different strain rates.
4. Dynamic initially unconfined with water in pressure cell, at two different strain rates.
5. Dynamic, initially confined, at two different confining pressures and two different strain rates.
6. Acoustic wave tests for wave speed determination.

All tests were performed on specimens with two sets of electrical resistance strain gages as shown in Figure 11. Each strain gage set consisted of a longitudinal and a transverse gage and denoted as Set A and Set B in a random manner. The data from each of the specimens are given below in the test summary of Table 3.

Table 3
Test Summary

Test	Description

1. QSM1 Quasistatic Mortar No. 1 Unconfined with load rate of 30 lbs/sec (133.4 N/sec) and a strain rate of approximately 1.2×10^{-6}/sec initially. Loaded to 18,000 lbs. (80.06 kN) in 10 min, held at 18,000 lbs (80.06 kN) for 10 min, unloaded to 12,000 lbs (53.38 kN) in 30 sec and reloaded to 18,000 lbs (80.06 kN) in 3.33 min. The stress-time plot for this test is given in Figure 12. The stress-strain plot for this test is shown in Figure 13. The young's modulus for the initial loading was measured at 3.63×10^{6} psi (25.0 GPa) and the loading-unloading modulus was measured at 3.61×10^{6} psi (24.90 GPa).
2. QSM3 Quasistatic Mortar No. 3. Load rate of 30 lbs/sec (133.4 N/sec) and strain rate of approximately 1.2×10^{-6}/sec. Loaded to failure with stress-strain curve in Figure 14. Longitudinal, transverse and volumetric strains shown in Figure 15. Hourglass type failure.
3. DCMU4 Direct Compression Mortar Unconfined No. 4 test in SHPB at a strain rate of approximately 60/sec. No confinement, specimen destroyed in multiple pieces. Axial compressive stress from transmitter bar shown in Figure 16. Two sets of longitudinal transverse and volumetric strains shown in Figures 17 and 18.
4. DCMU5 Direct Compression Mortar Unconfined No. 5 test SHPB at a strain rate of approximately 160/sec. No confinement, specimen destroyed in multiple pieces. Axial

UNCONFINED MORTAR QUASISTATIC TEST

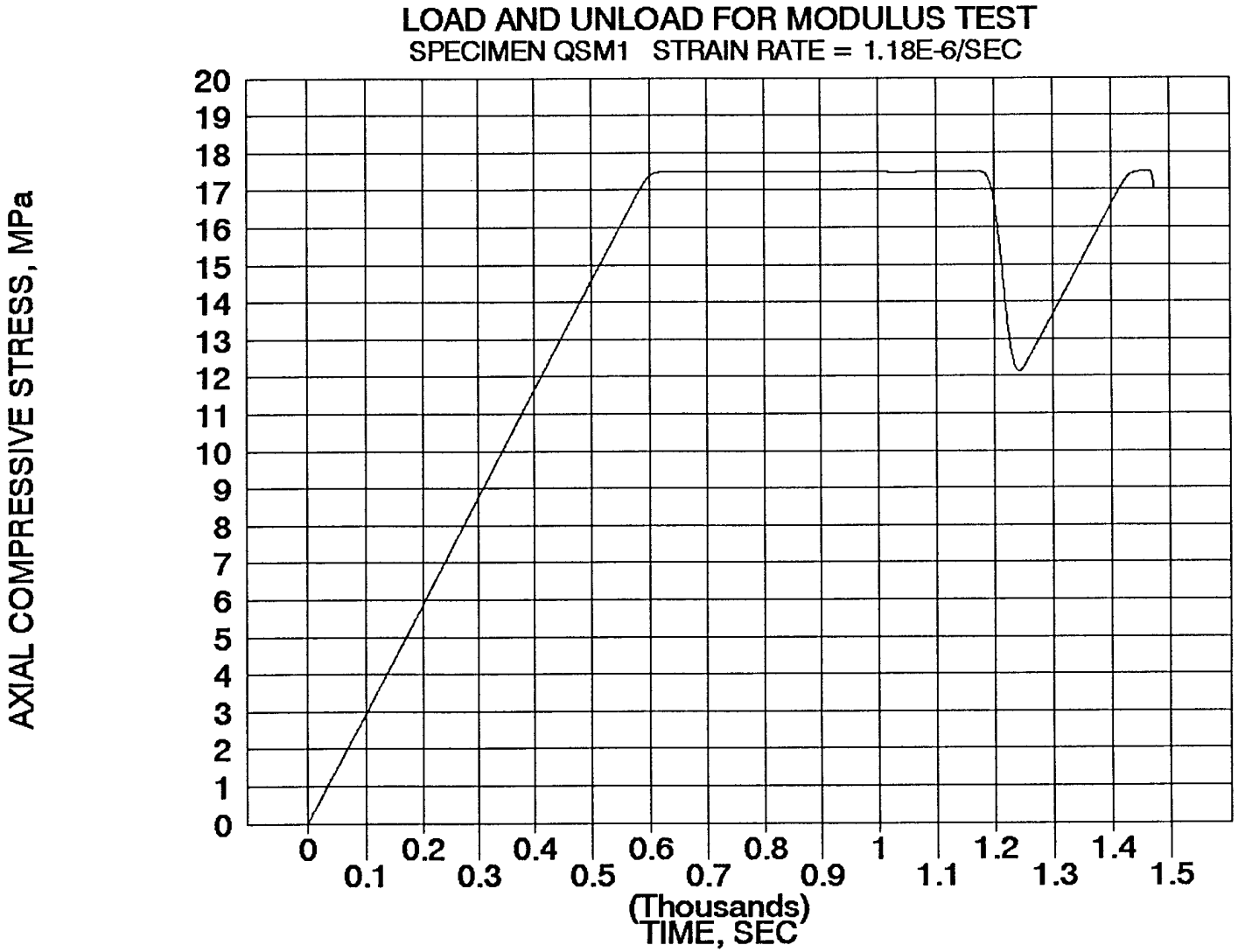

Figure 12. Stress-time curve for determning the modulus of mortar.

UNCONFINED MORTAR QUASISTATIC TEST

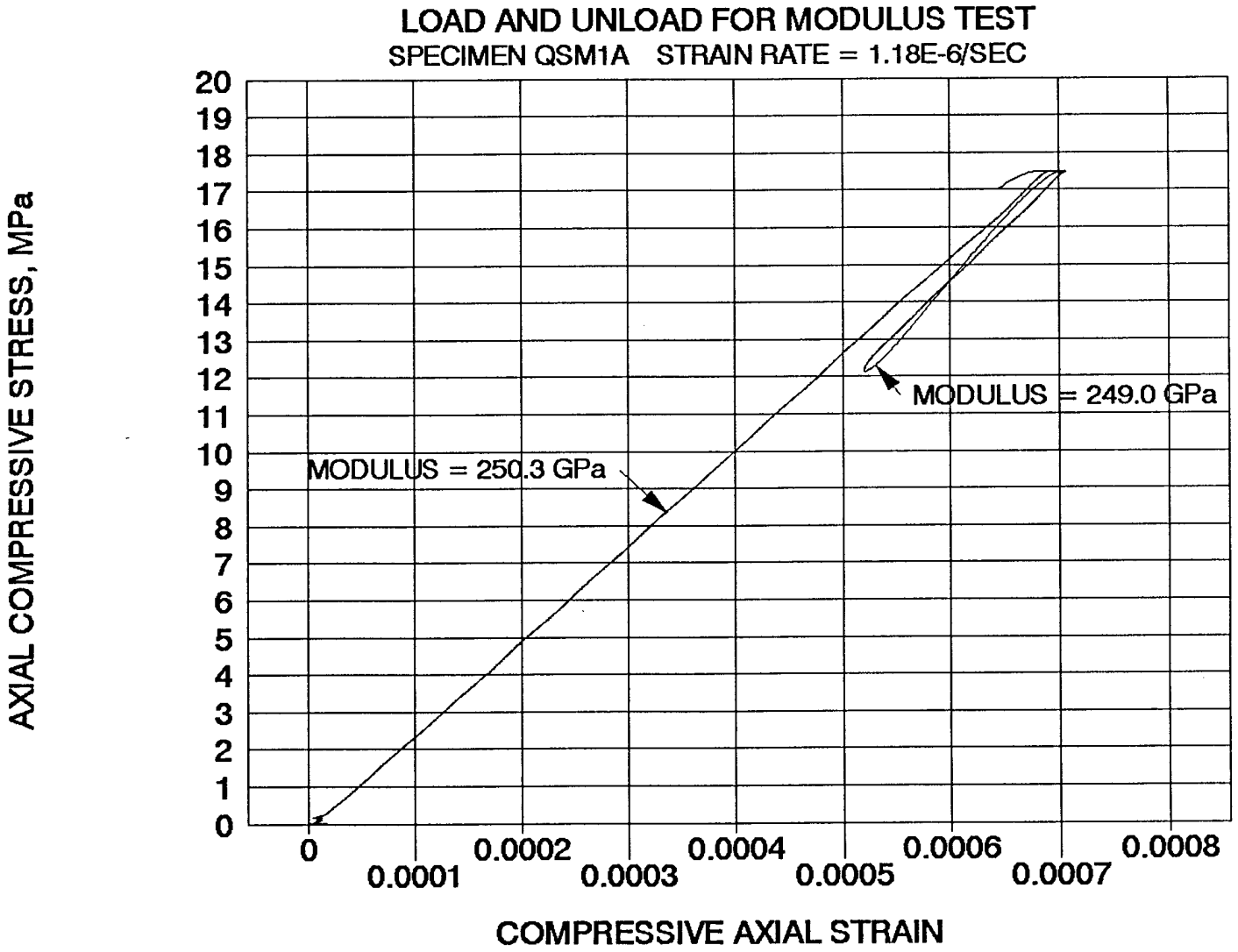

Figure 13. Stress-strain curve of loading and unloading for determining the modulus of mortar.

UNCONFINED MORTAR QUASISTATIC TEST

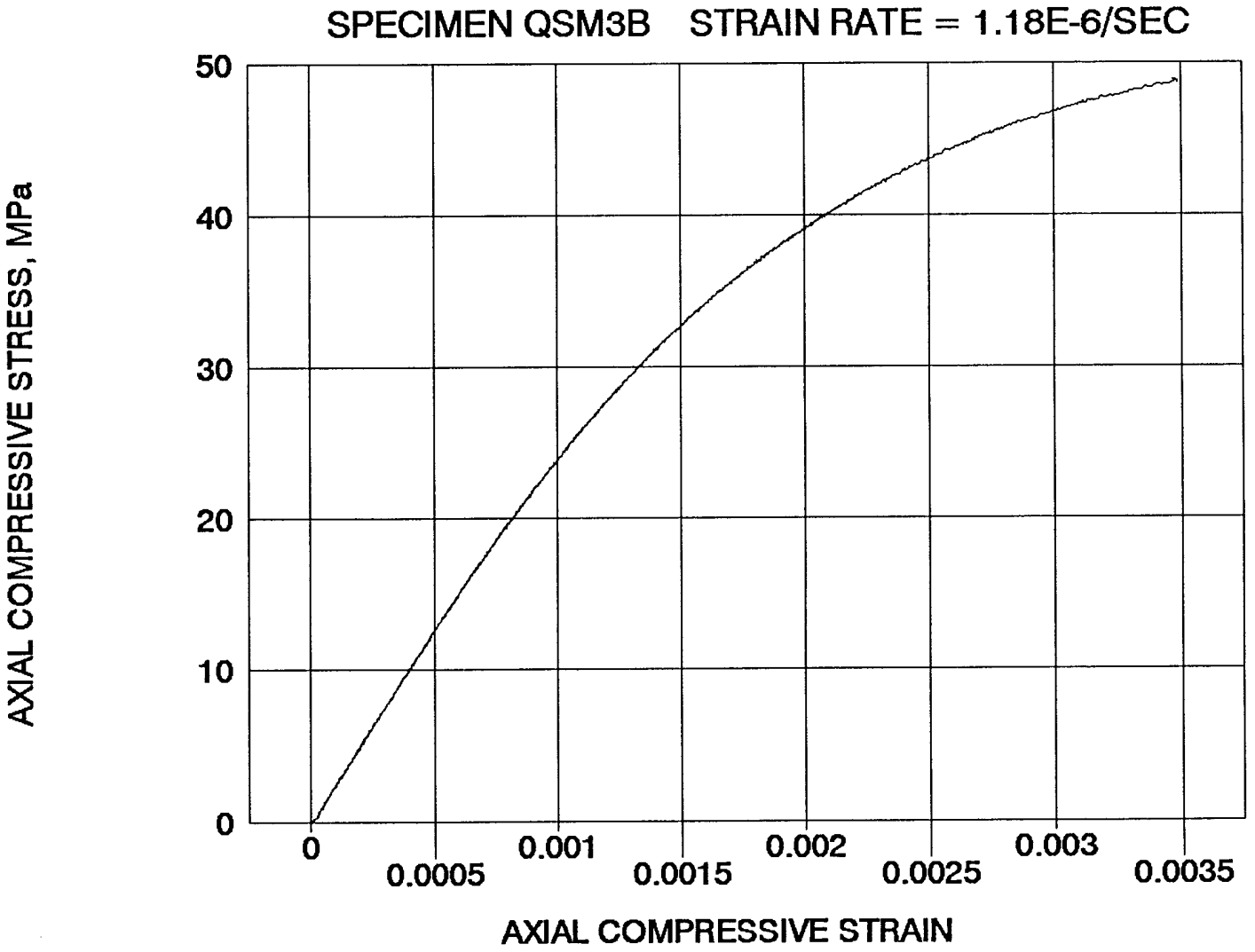

Figure 14. Stress-strain curve for mortar.

UNCONFINED MORTAR QUASISTATIC TEST

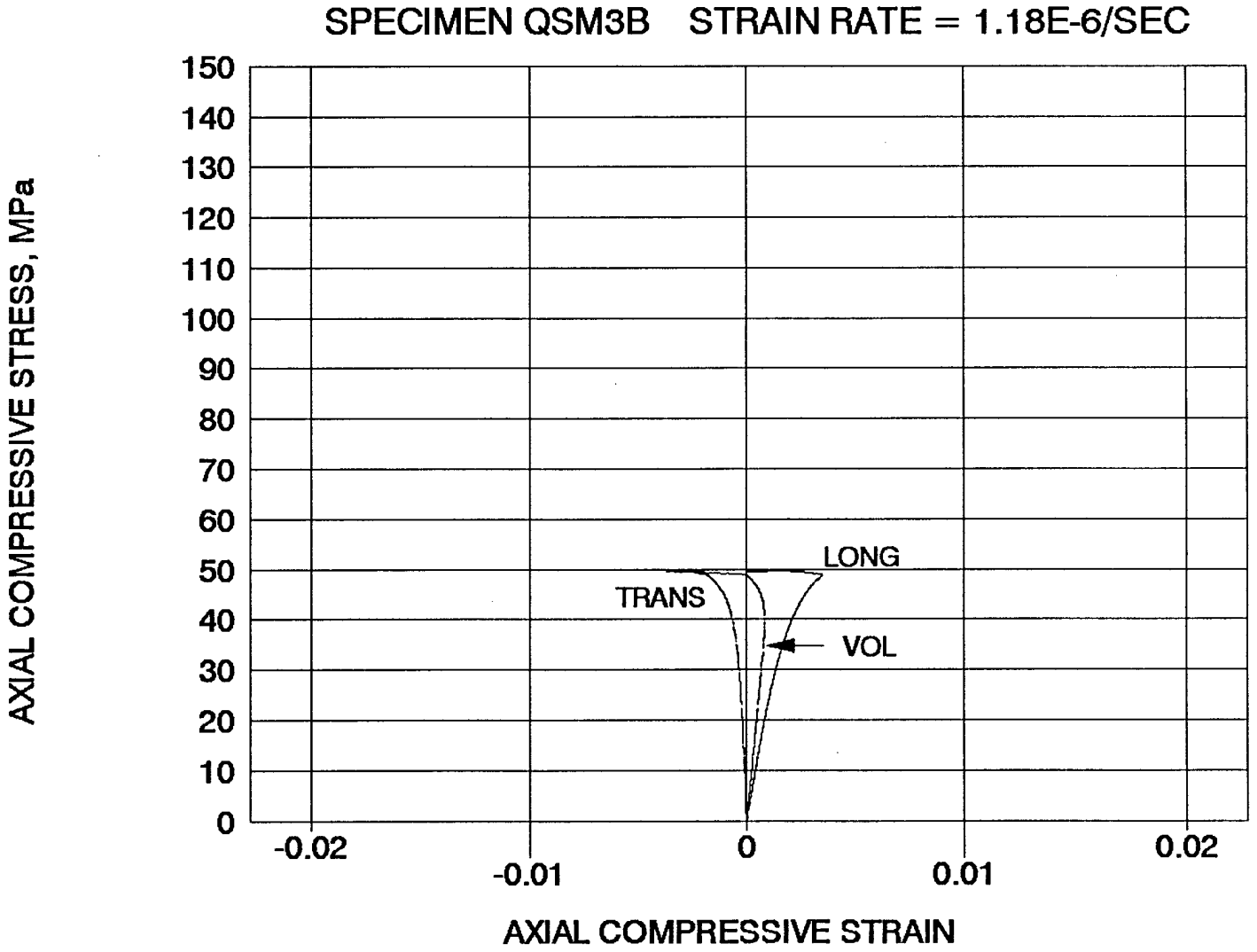

Figure 15. Longitudinal, transverse and volumetric strains for one set of strain gages for QSM3.

UNCONFINED MORTAR TEST IN SHPB

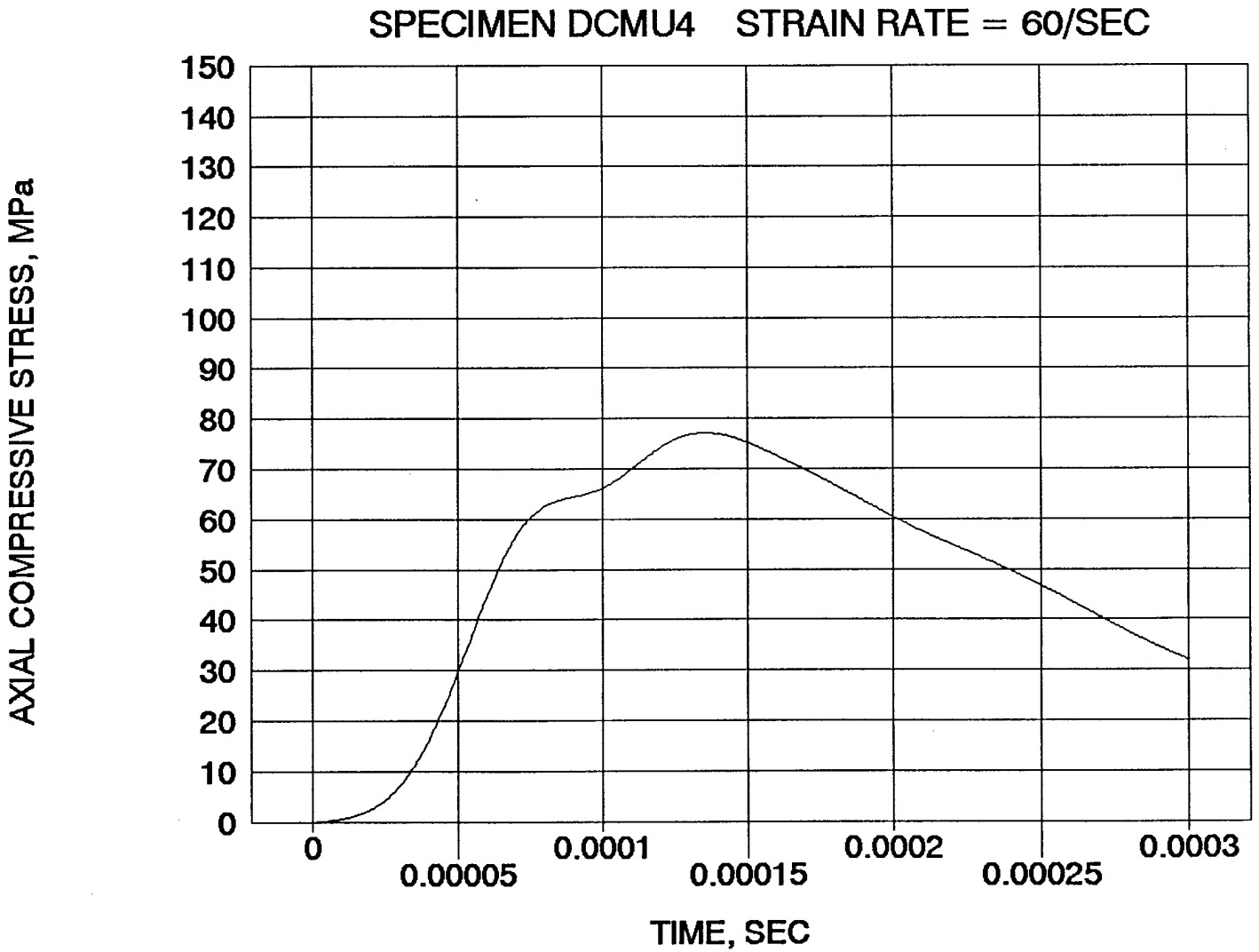

Figure 16. Axial load (transmitted stress) for DCMU4. No confining pressure.

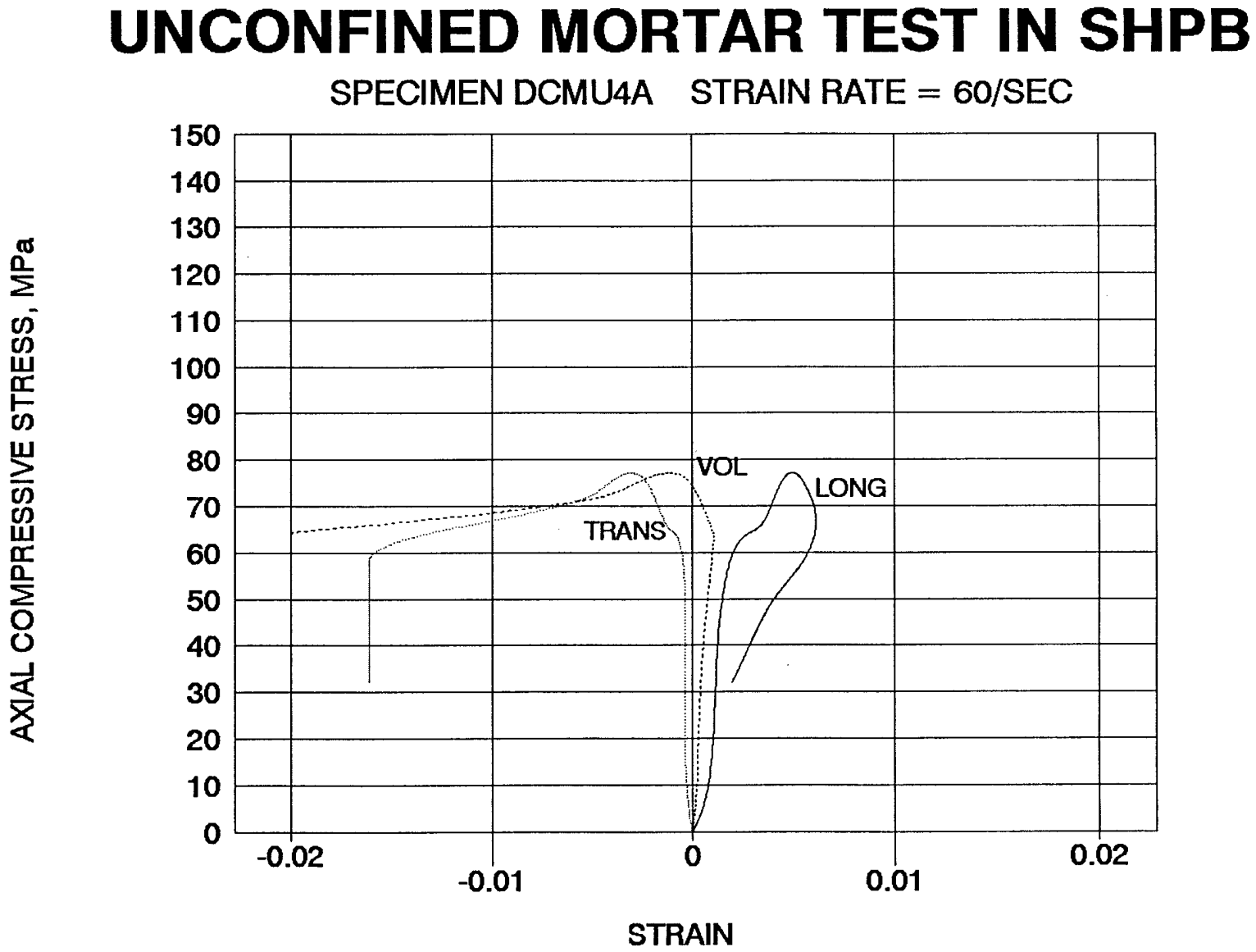

Figure 17. Longitudinal, transverse and volumetric strains for one strain gage set of DCMU4.

UNCONFINED MORTAR TEST IN SHPB

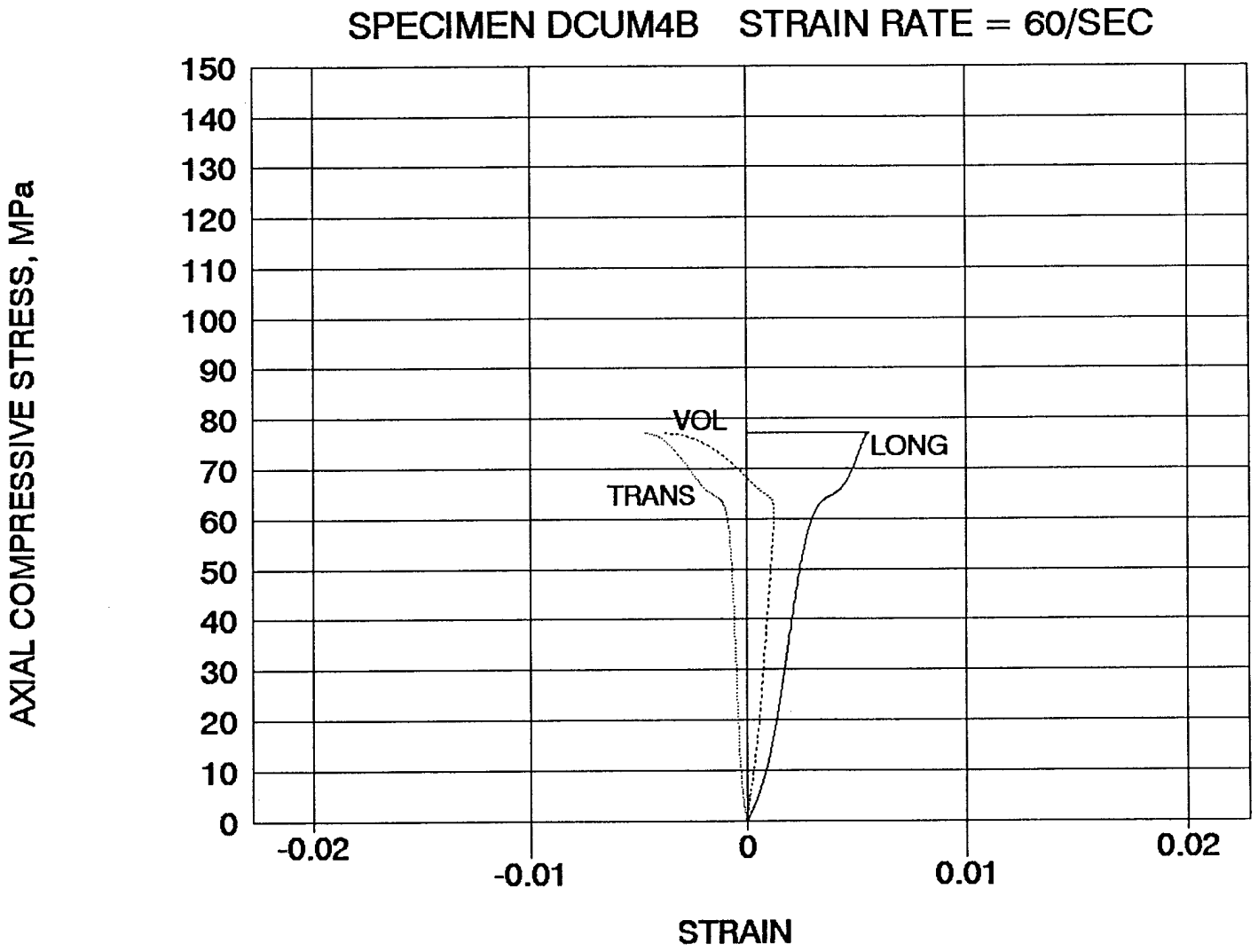

Figure 18. Longitudinal, transverse and volumetric strains for the second set of strain gages for DCMU4.

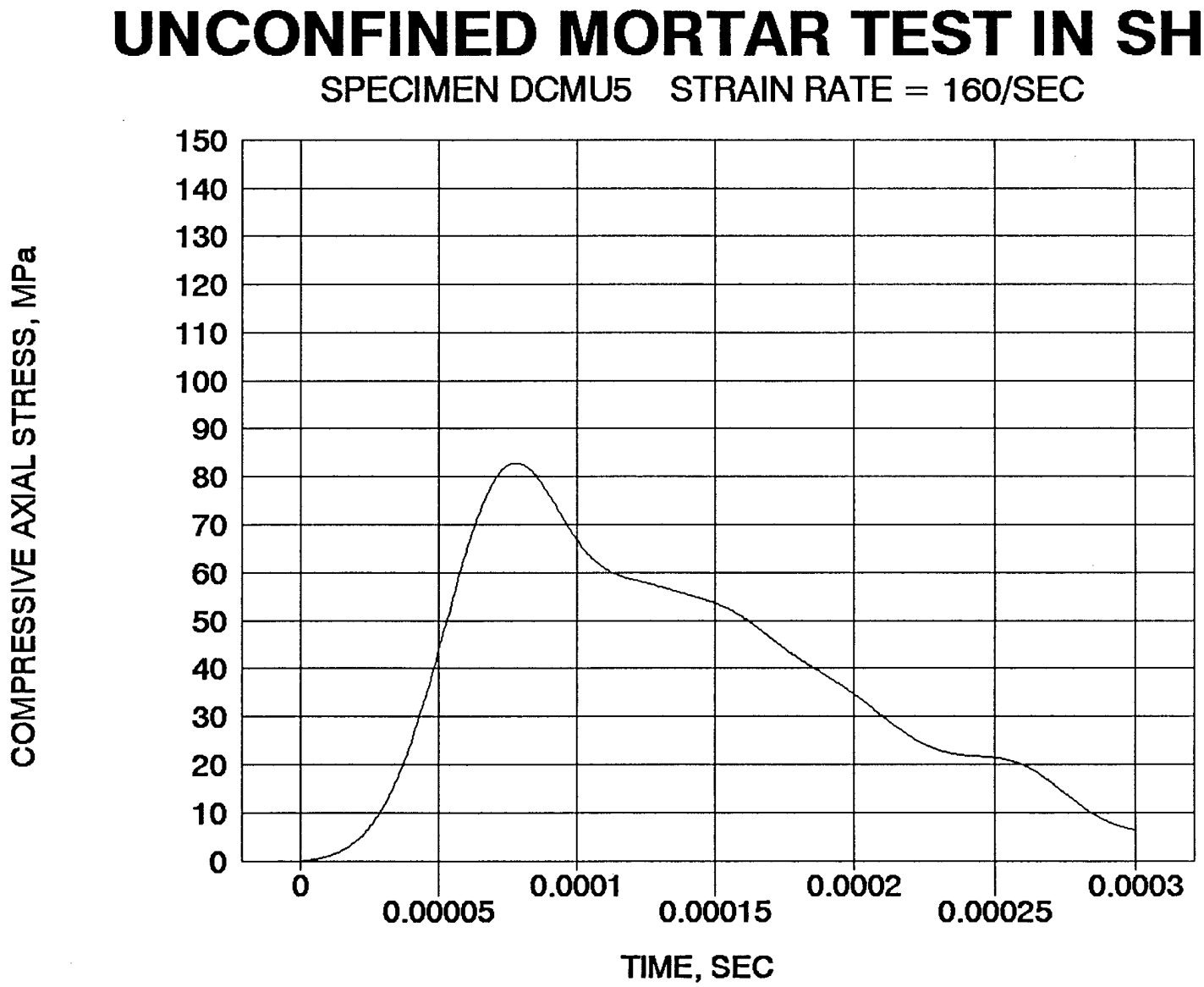

Figure 19. Axial load (transmitted stress) for DCMU5. No confining pressure.

UNCONFINED MORTAR TEST IN SHPB

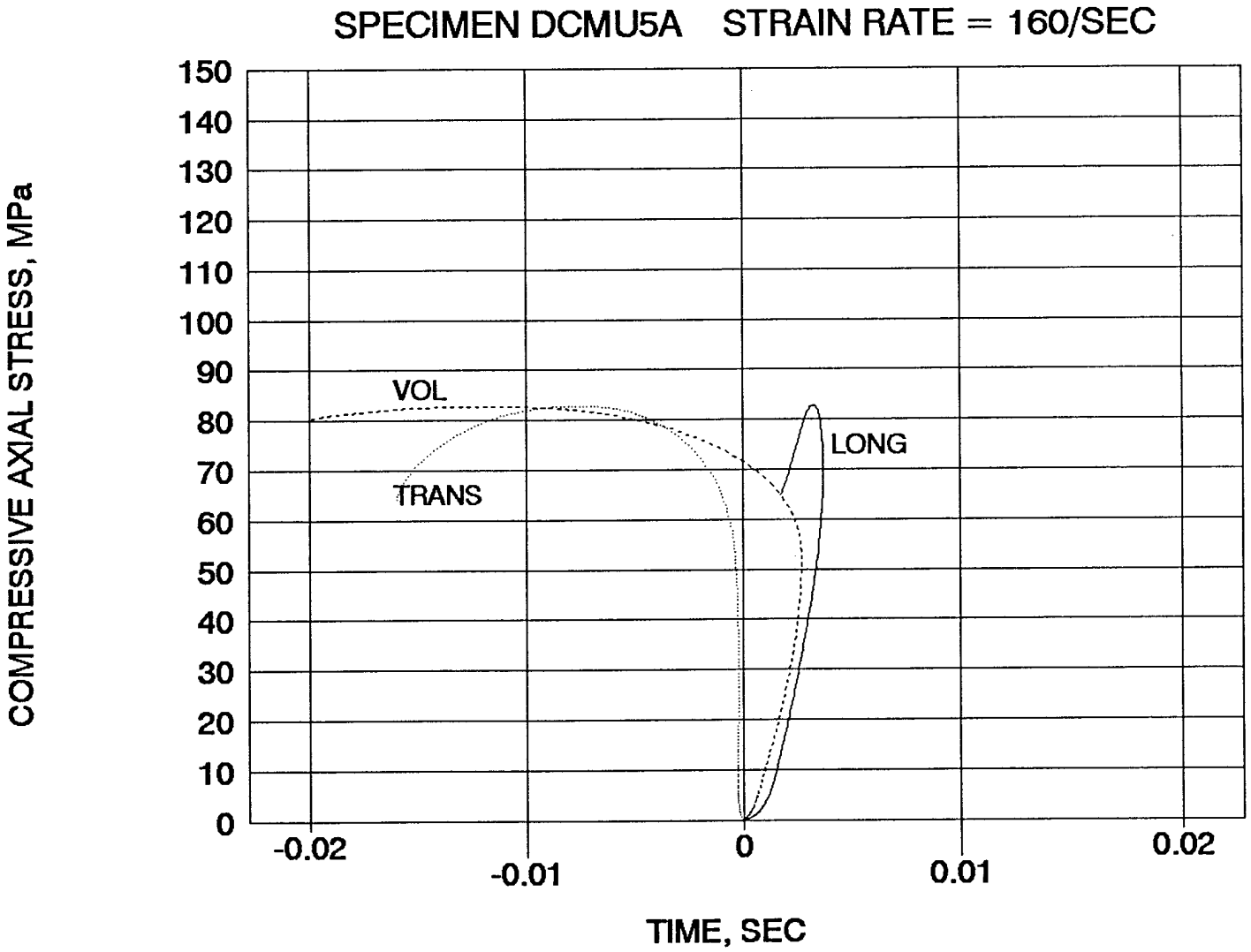

Figure 20. Longitudinal,transverse and volumetrioc strains for one strain gage set of DCMU5.

UNCONFINED MORTAR TEST IN SHPB

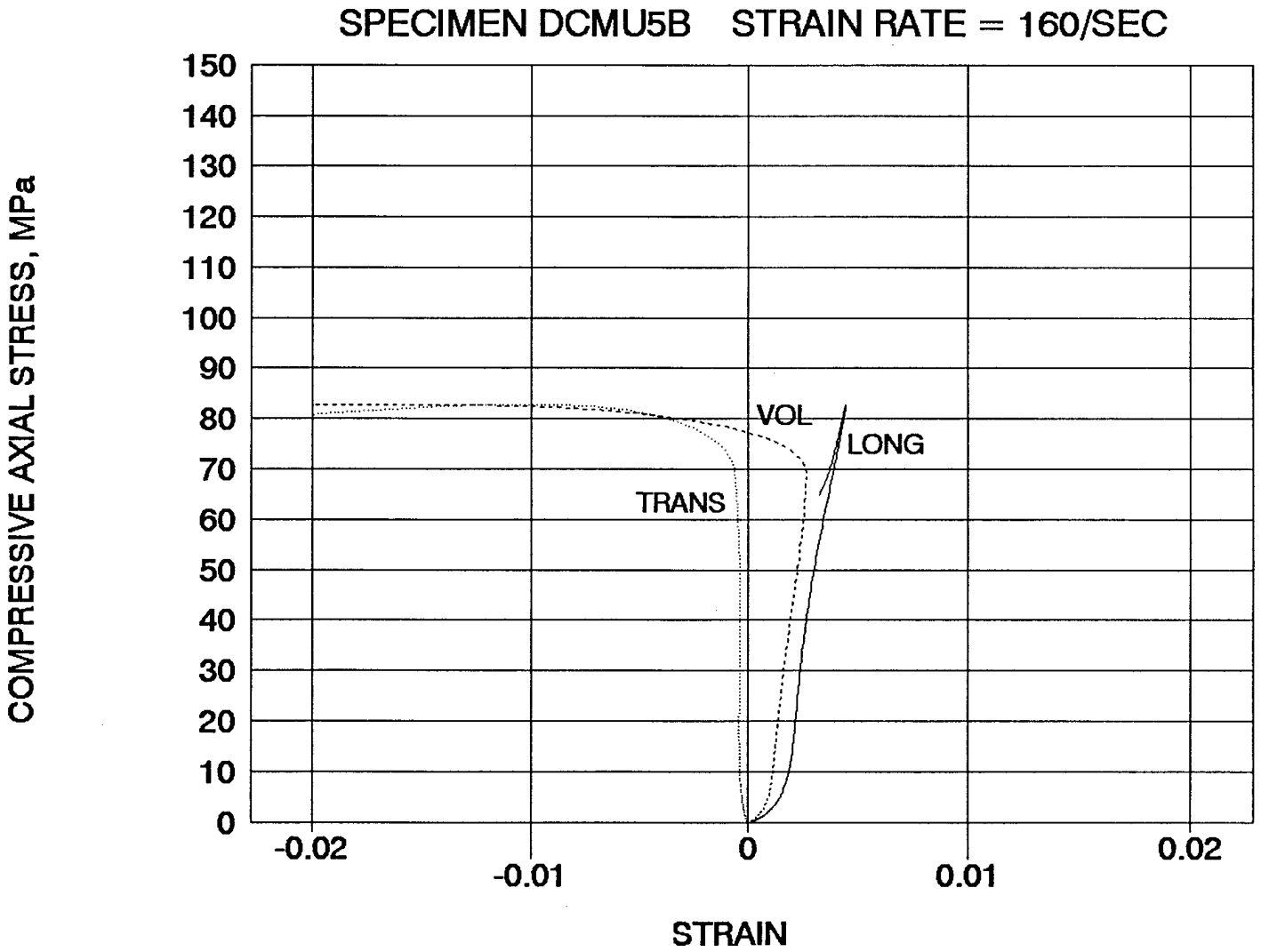

Figure 21. Longitudinal, transverse, and volumetric strains for the second set of strain gages for DCMU5.

compressive stress from the transmitter bar shown in Figure 19. Two sets of longitudinal , transverse and volumetric strains shown in Figures 20 and 21.

5. DCMC5 Direct Compression Mortar Confined No. 5 SHPB test in SHPB at a strain rate of approximately 60/sec. Initial confining pressure of zero with pressure cell filled with water. Specimen showed multiple longitudinal cracks but intact. Axial compressive stress from the transmitter bar and the confining pressure from pressure cell are shown in Figure 22. Two sets of longitudinal transverse and volumetric strains shown in Figures 23 and 24.

6. DCMC10 Direct Compression Mortar Confined Test No. 10 in SHPB at a strain rate of approximately 125/sec. Initial confining pressure of 460 psi. Specimen showed light longitudinal cracking but remained solid and intact. Axial compressive stress from transmitter bar and confining pressure in pressure cell shown in Figure 25. One set of longitudinal, transverse and volumetric strains shown in Figure 26.

7. DCMC11 Direct Compression Mortar Confined No. 11 in SHPB at a strain rate of approximately 140/sec. Initial confining pressure of zero with pressure cell filled with water. Specimen showed multiple cracks but intact. Axial compressive stress from transmitter bar and confining pressure from pressure cell shown in Figure 27. Two sets of longitudinal, transverse and volumetric strains shown in Figures 28 and 29.

8. DCMC12 Direct Compression Mortar Confined No. 12 in SHPB at a strain rate of approximately 120/sec. Initial confining pressure of 960psi. Specimen showed no visible damage. Axial compressive stress from transmitter bar and confining pressure from pressure cell shown in Figure 30. Two sets of longitudinal, transverse and volumetric strains shown in Figures 31 and 32.

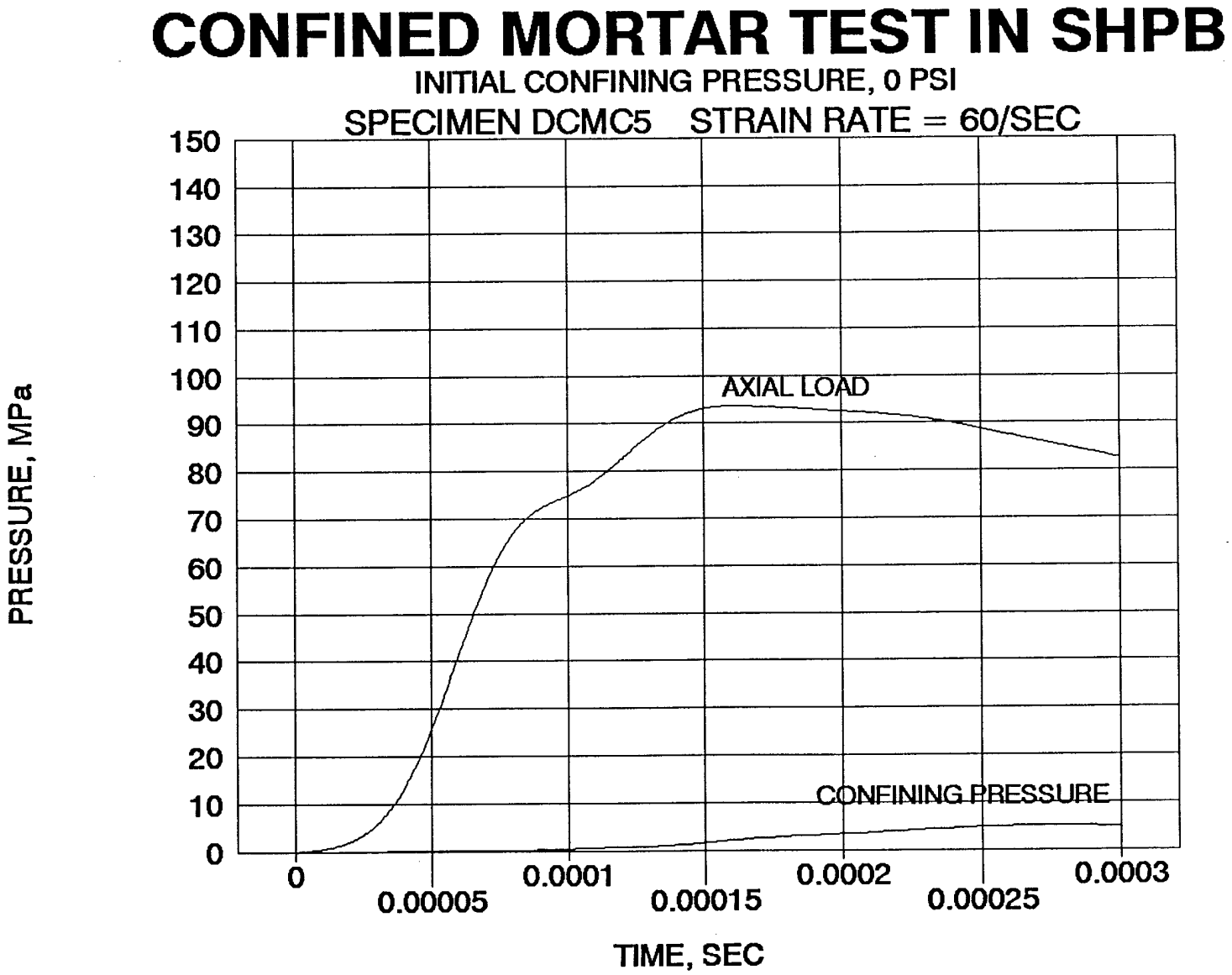

Figure 22. Axial load (transmitted stress) and confining pressure for DCMC5.

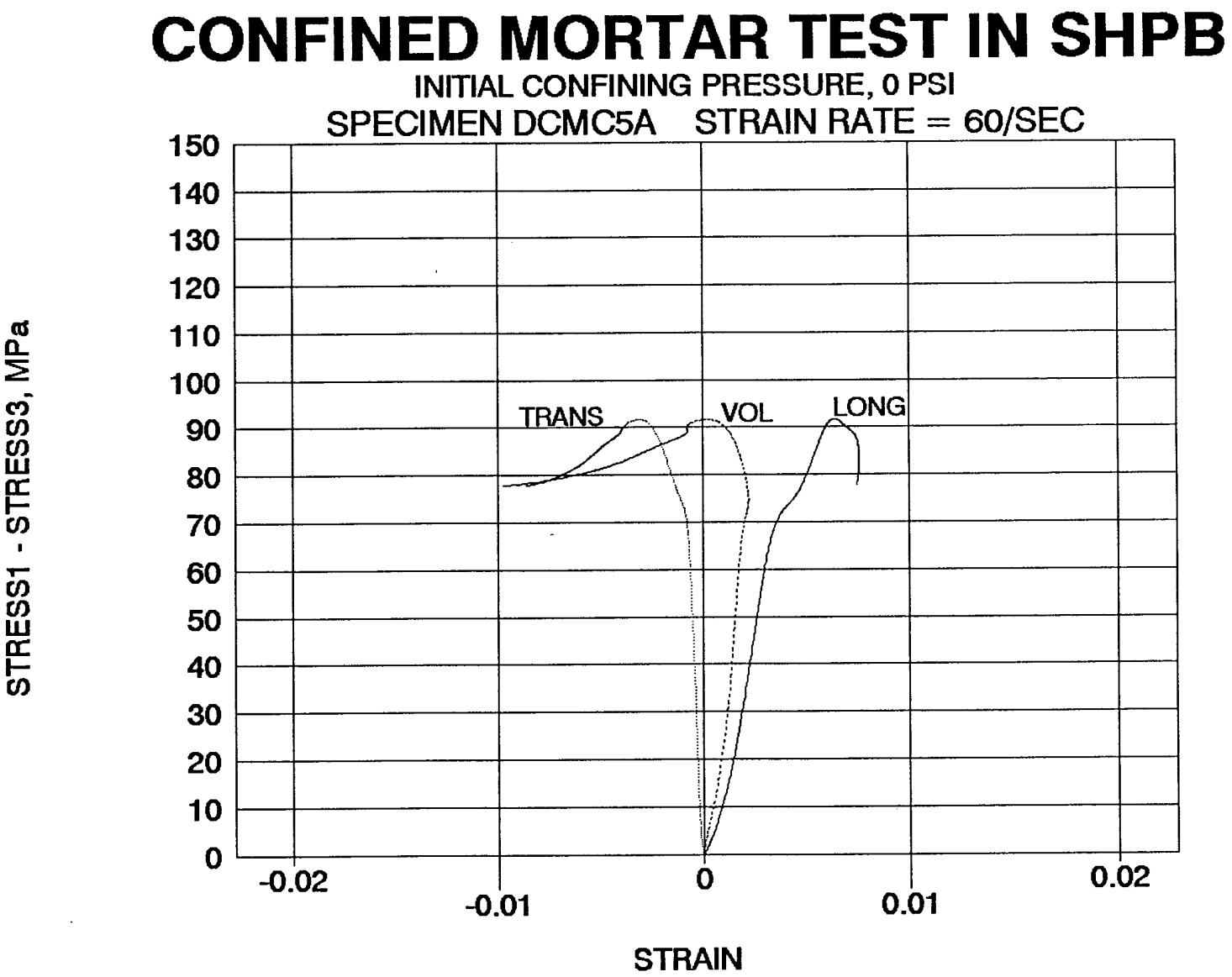

Figure 23. Longitudinal, transverse and volumetric strains for one strain gage set of DCMC5.

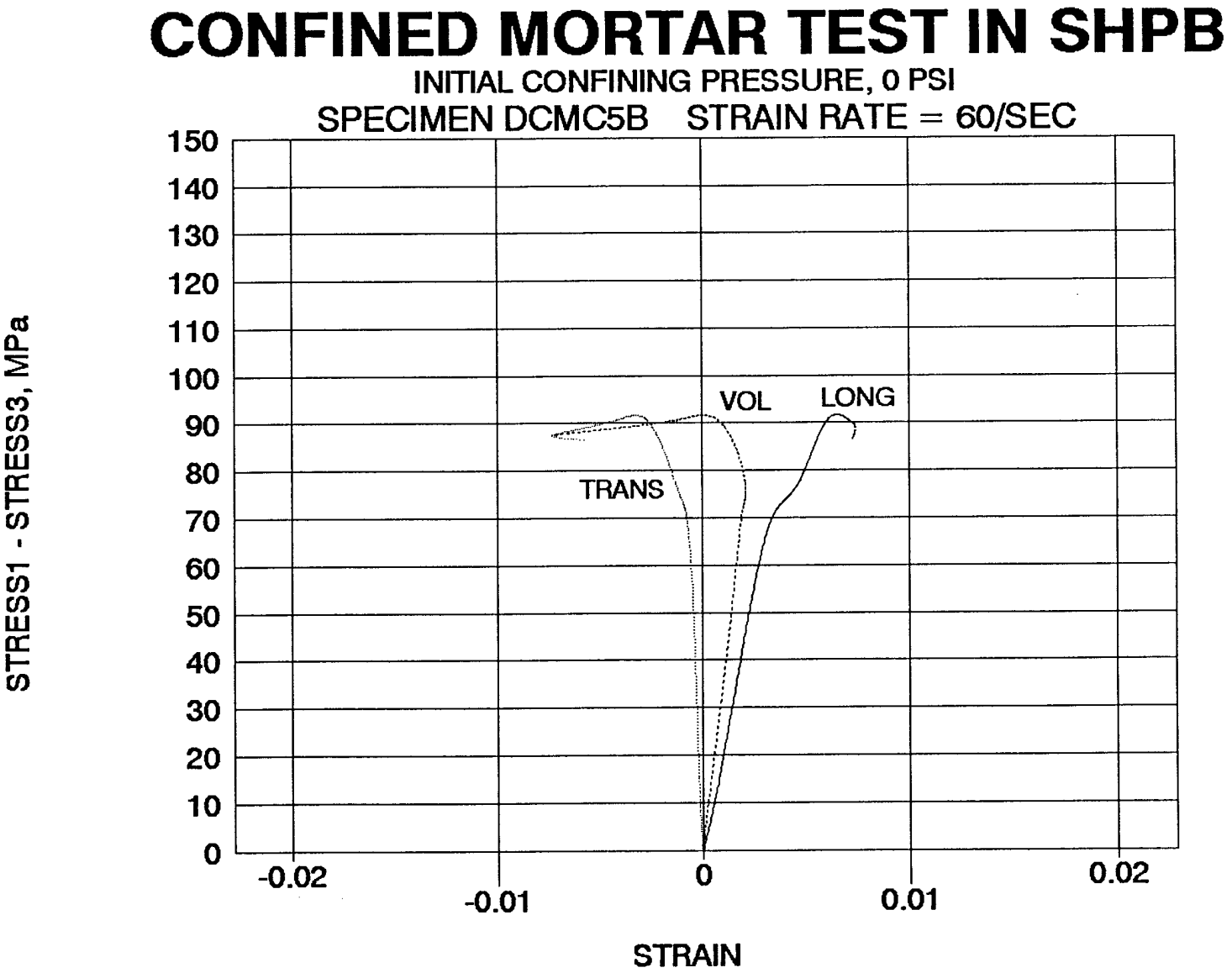

Figure 24. Longitudinal, transverse and volumetric strains for the second set of strain gages for DCMC5.

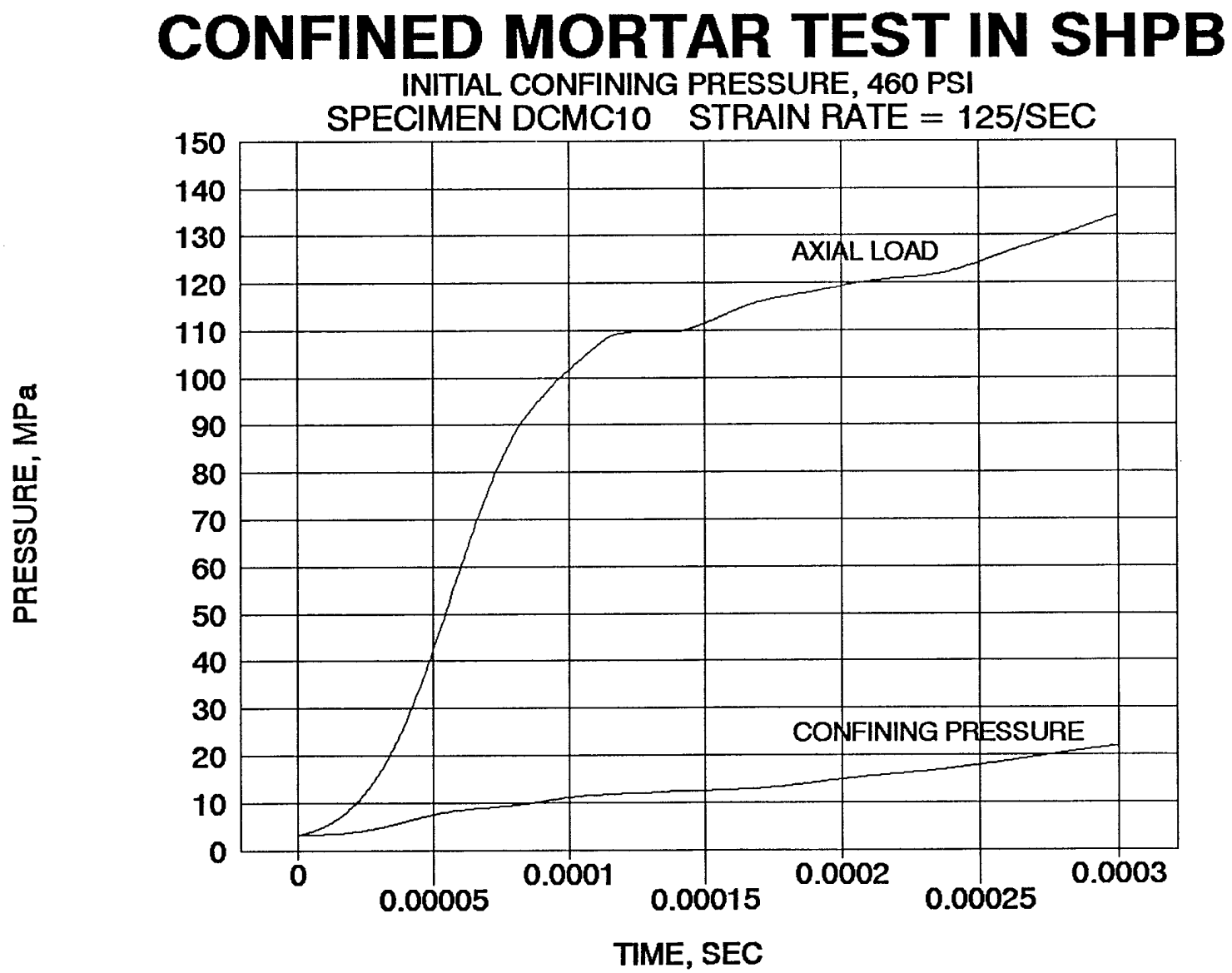

Figure 25. Axial load (transmitted stress) and confining pressure for DCMC10.

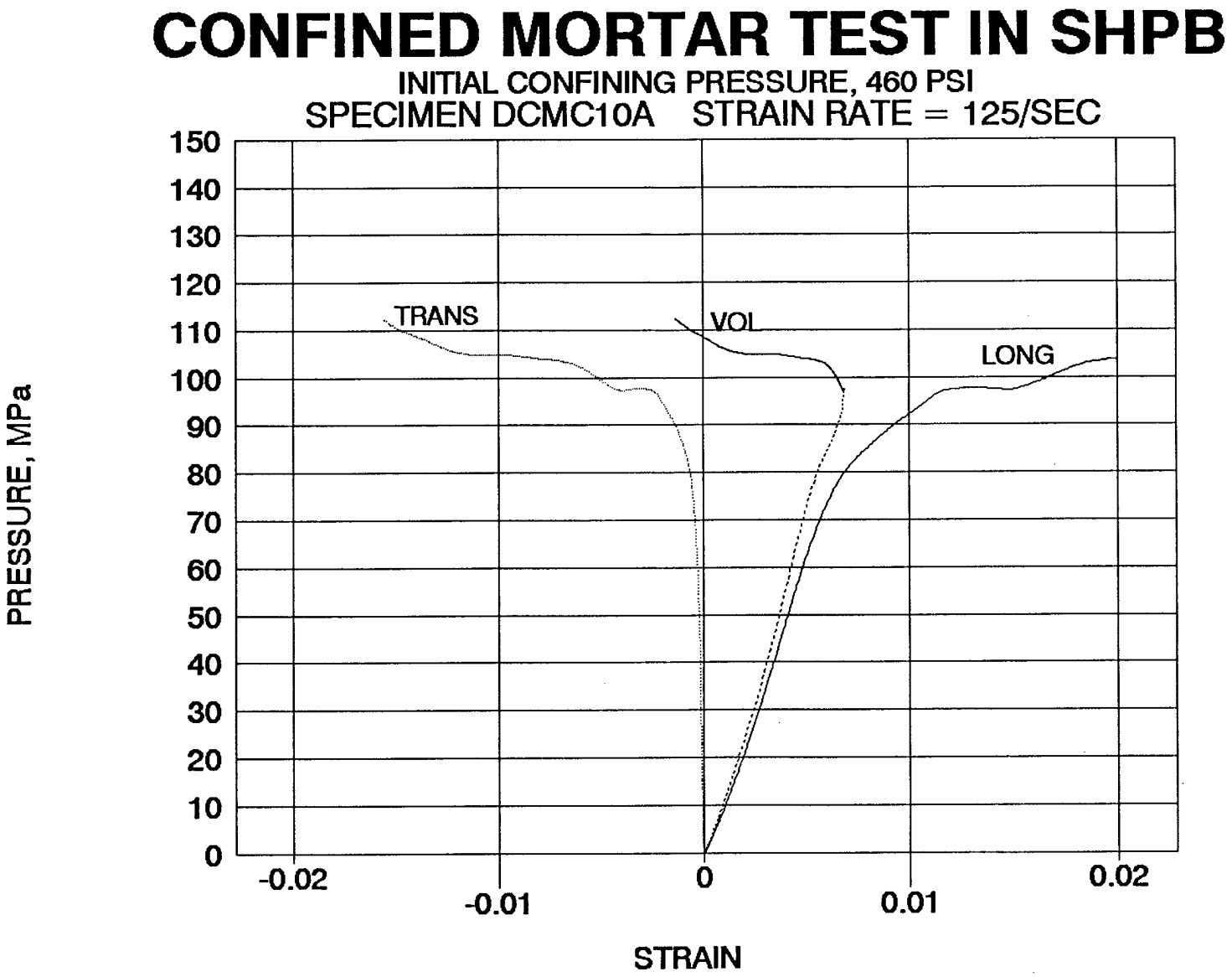

Figure 26. Longitudinal, transverse and volumetric strains for one strain gage set of DCMC10. Other set of data not usuable.

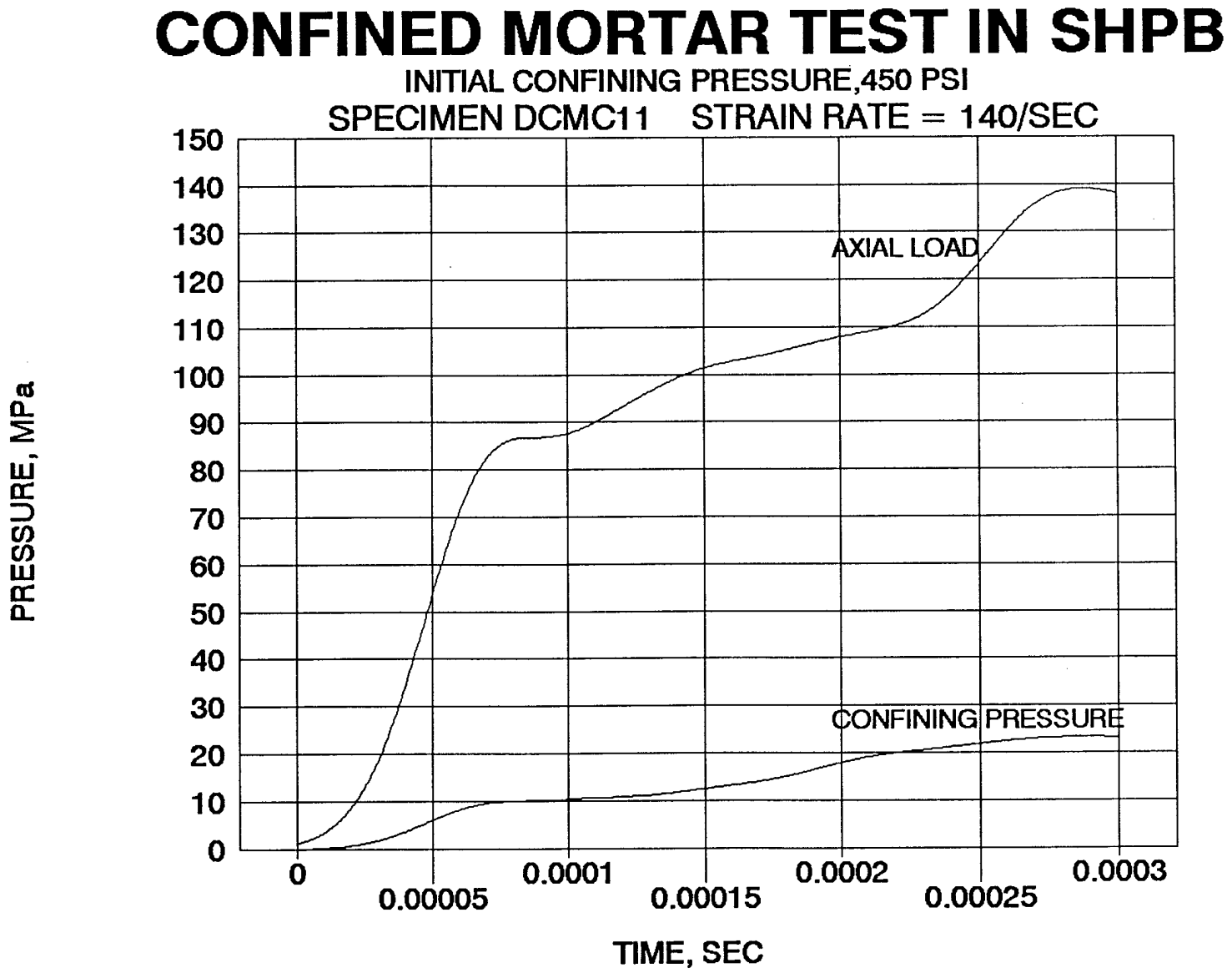

Figure 27. Axial load (transmitted stress) and confining pressure for DCMC11.

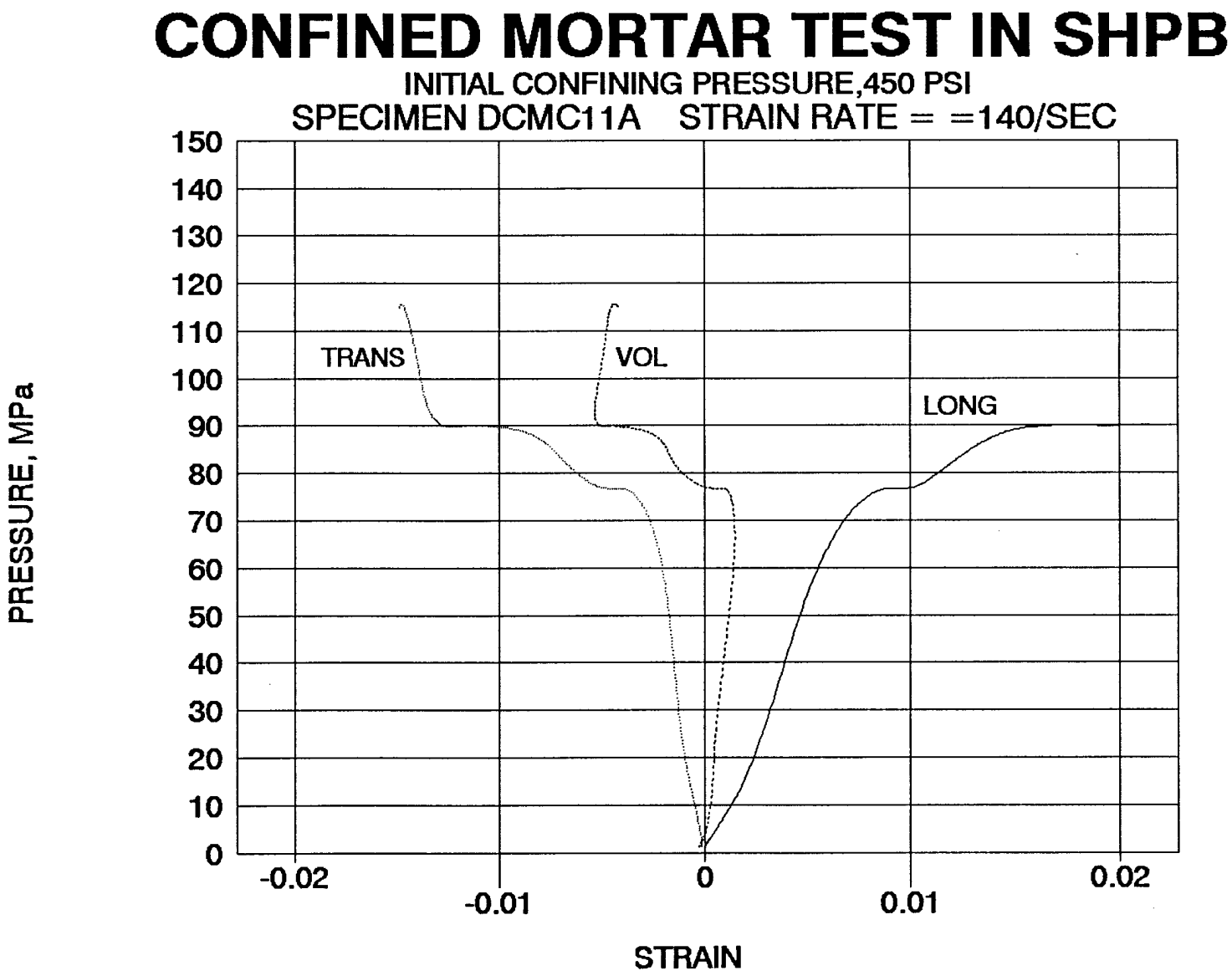

Figure 28. Longitudianl, transverse and volumetric strains for one strain gage set of DCMC11.

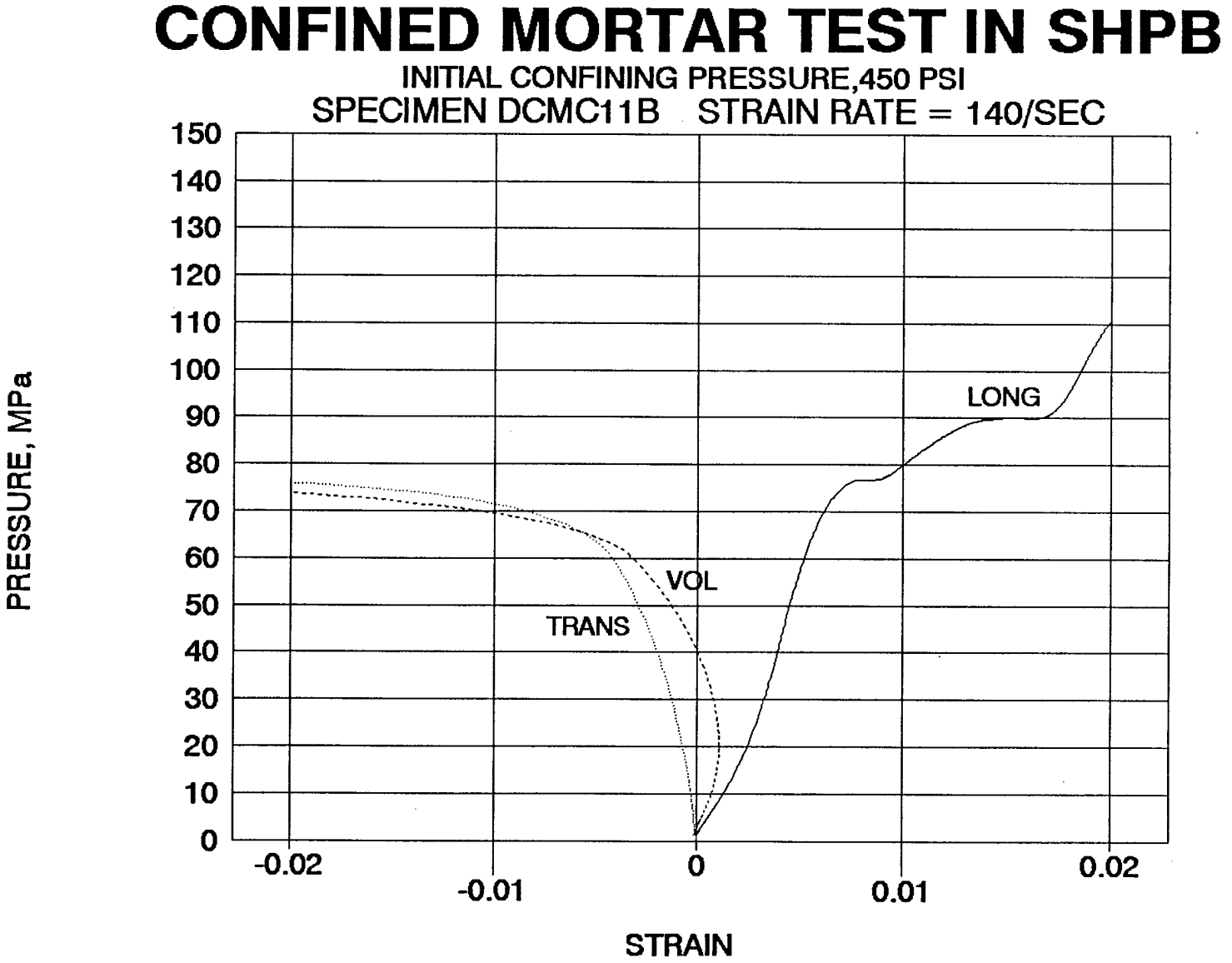

Figure 29. Longitudinal, transverse and volumetric strains for the second set of strain gages for DCMC11.

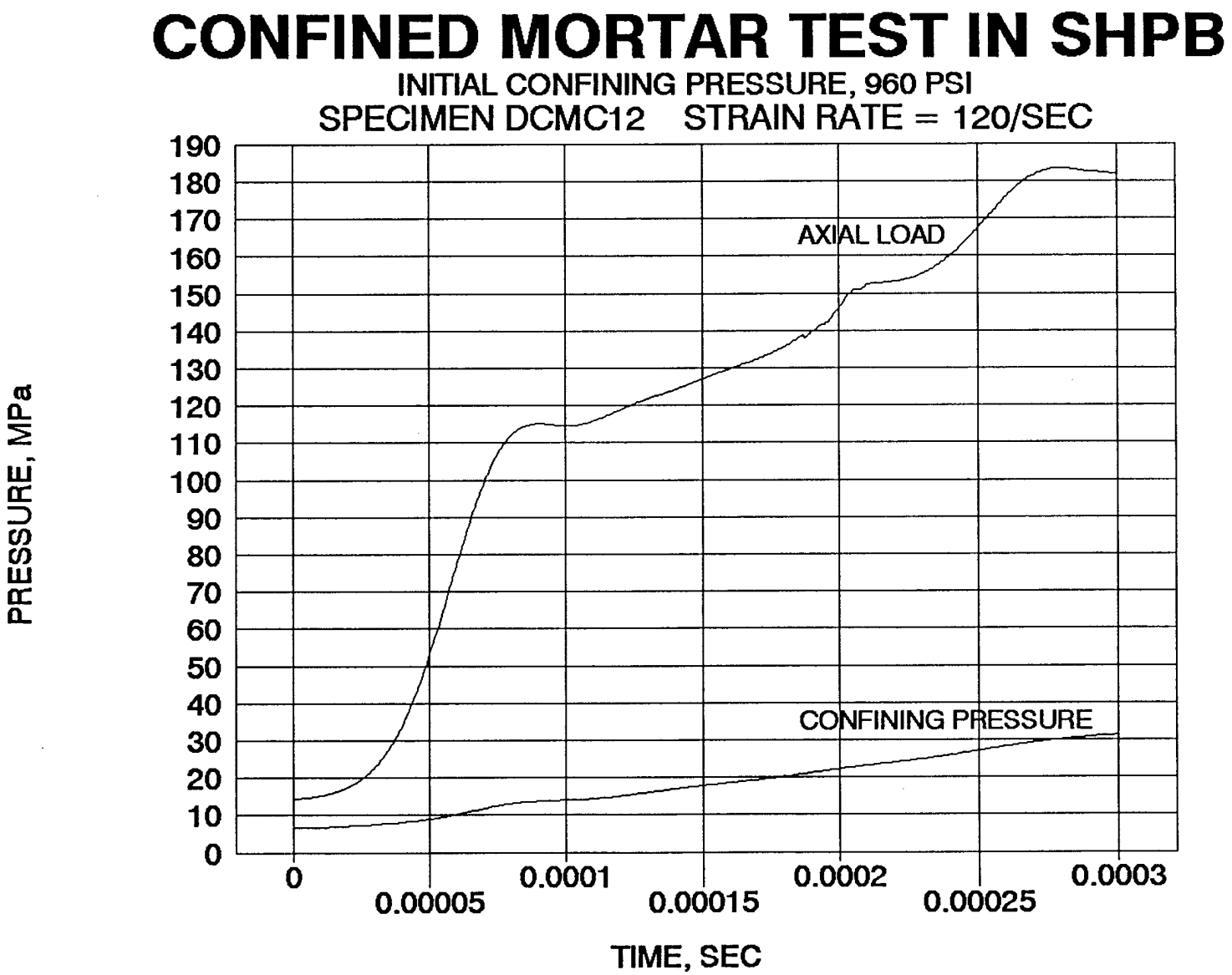

Figure 30. Axial load (transmitted stress) and confining pressure for DCMC12.

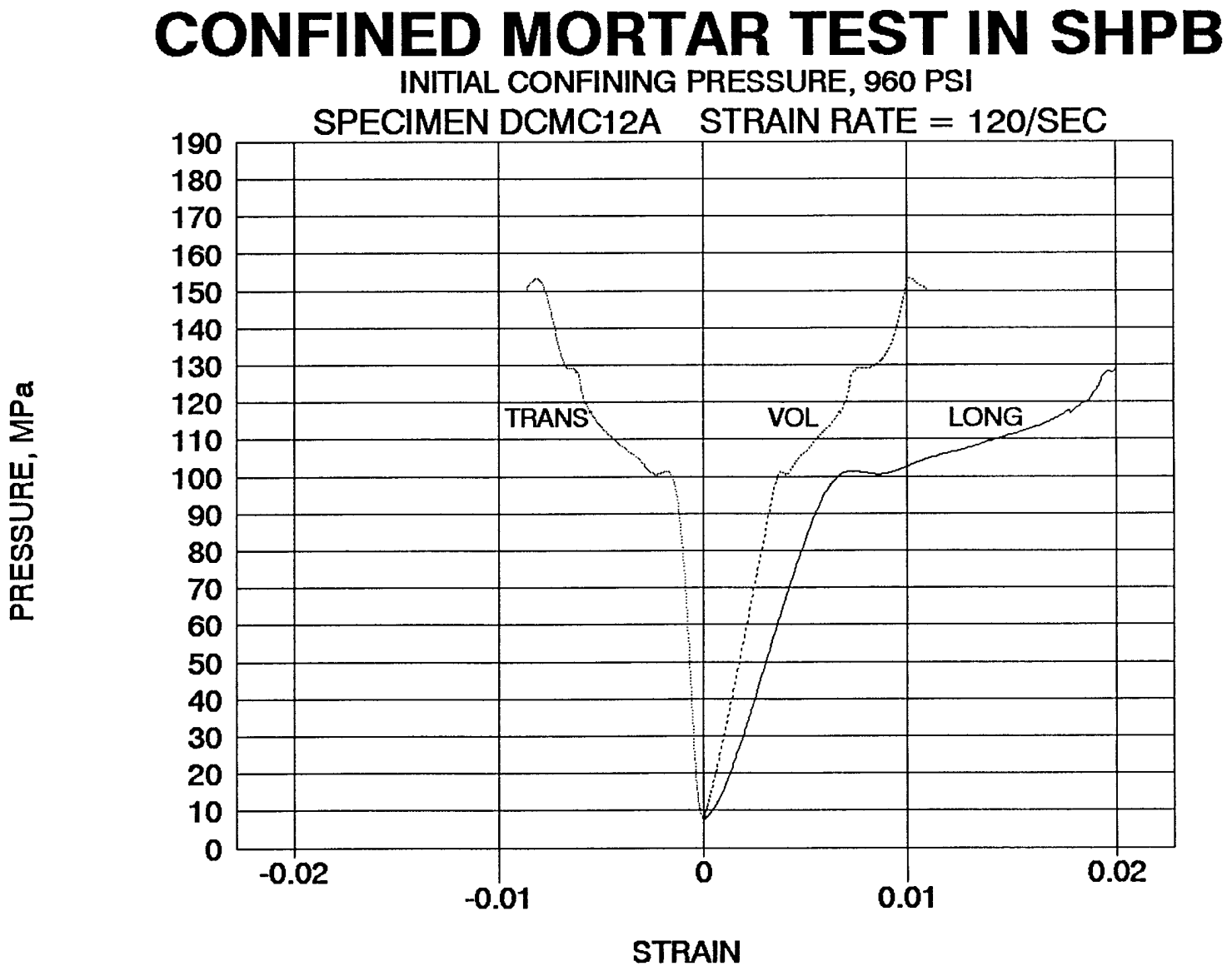

Figure 31. Longitudinal, transverse and volumetric strains for on strain gage set of DCMC12.

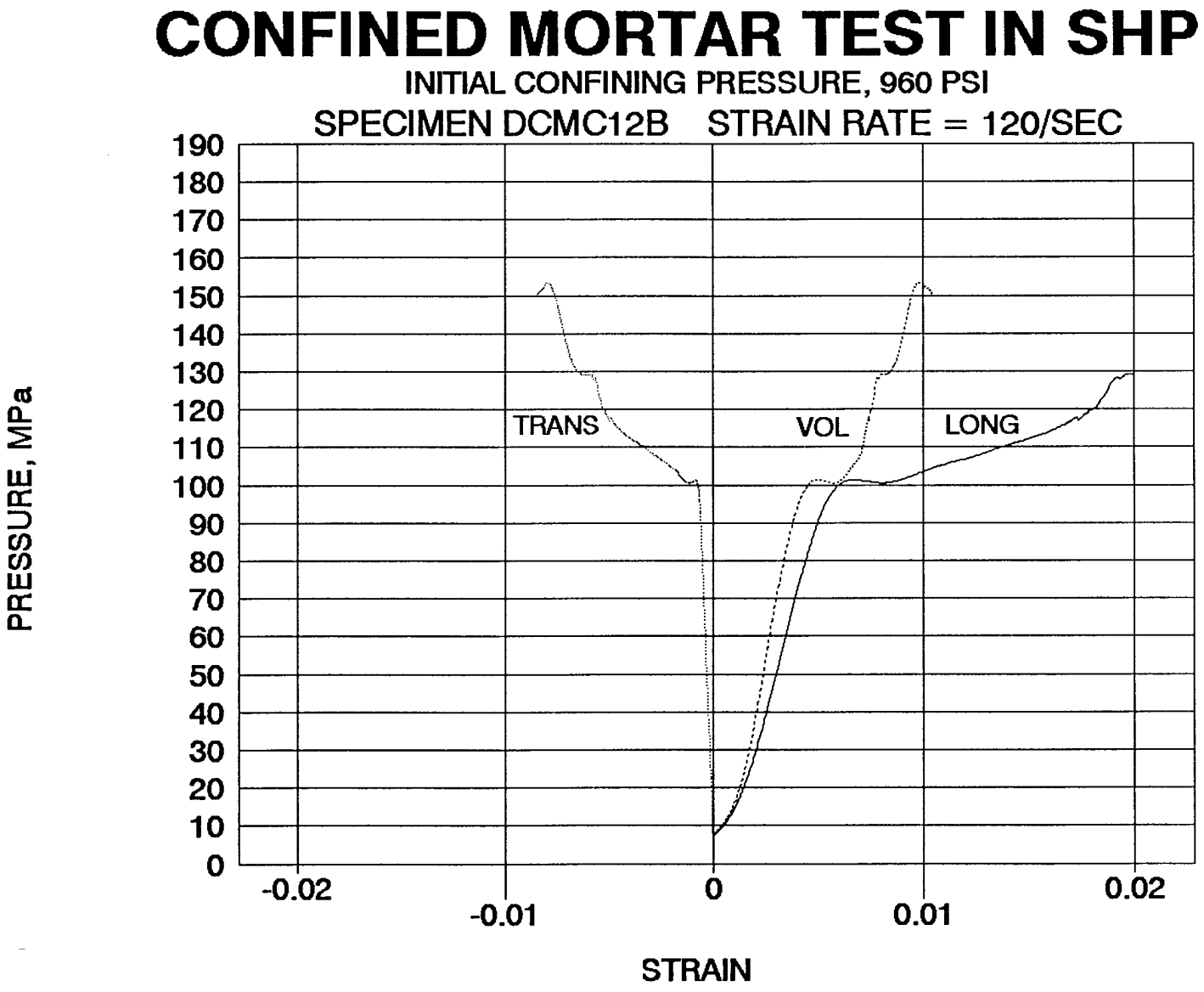

Figure 32. Longitudinal, transverse and volumetric strains for the second set of strain gages for DCMC12.

9. Acoustic Tests Ten specimens were measured, weighed, and tested with an acoustic transducer to determine the wave speed of the mortar. A velocity meter using a small diameter (19mm) 150 kHz transducer was used for longitudinal wave speed measurement. The transducers were placed at positions C and C^1 of Figure 11. The average wave speed was determined to be 3.92 km/sec. Since the transducer was small compared to the specimen size it was assumed that the wave speed was of the unbounded type and for a Poisson's ratio of 0.2 the Young's modulus was calculated at 28.73 GPa (4.17×10^6 psi), which doesn't agree all that well with the value of 24.97 GPa (3.62×10^6 psi) measured in the quasistatic load tests. Assuming higher modes for the longitudinal waves may predict a phase velocity on the order of the measured velocity.

4. Discussion

For the data presented in the previously referenced figures of the unconfined tests, the strains are plotted versus the axial stress and for data from confined tests the strains are plotted versus Stress 1 minus Stress 3. Stress 1 is the axial stress and Stress 3 is the confining pressure.

Both longitudinal strain ε_L and transverse strain ε_T signals are collected directly from the specimen and the volumetric strain ε_V is calculated using the following equation

$$\varepsilon_V = \varepsilon_L + 2\,\varepsilon_T \qquad (3)$$

This relation is based on the assumption that the radial and transverse strains are equal for a cylindrical specimen. For compressed rock and concrete, as loading is increased an initial compression occurs and a Poisson effect produces a small transverse strain but as the loading increases cracking and swelling occur and this is termed dilatancy. An indication of dilatancy is the change of sign of the volumetric strain. Dilatancy is seen to occur for all specimens tested, except for the dynamic test at the highest strain rate and highest confining pressure. (See Figures 31 and 32). The increase in the volumetric strain is quite evident when comparing the volumetric

strains of the quasistatic loading in Figure 15 and the dynamic unconfined test of Figures 17 and 18. Also an increase in the volumetric strain is evident between the unconfined SHPB tests at strain rate of 60/sec of Figure 17 and a similar test at a strain rate of 160/sec Figure 21. This also appears to be true for the confined SHPB tests, however at the highest confined SHPB test of Figures 31 and 32, even though the volumetric strain increased significantly it did not change sign with any evidence of dilatancy. This is probably attributed to the fact that loading pulse only lasts a finite time and did not have sufficient energy to overcome the high confining pressure. To make an easier comparison of effects of strain rate on the volumetric strain for some unconfined tests Figure 33 is given showing volumetric strain versus axial stress for three different strain rates. Also, Figure 34 shows some effect of strain rate, for confined tests, on volumetric strain versus the difference of principal stresses.

The effects of confinement on the dynamic compressive strength is very interesting. In all of the SHPB tests conducted, the confining pressure was no more than approximately ten percent of the axial load, but in all cases it was sufficient to cause considerable strain hardening and in most all cases was sufficient to prevent catastrophic failure of the specimen. It is recommended that a study be conducted to determine a measure of damage relative to amount of confining pressure present in the tests.

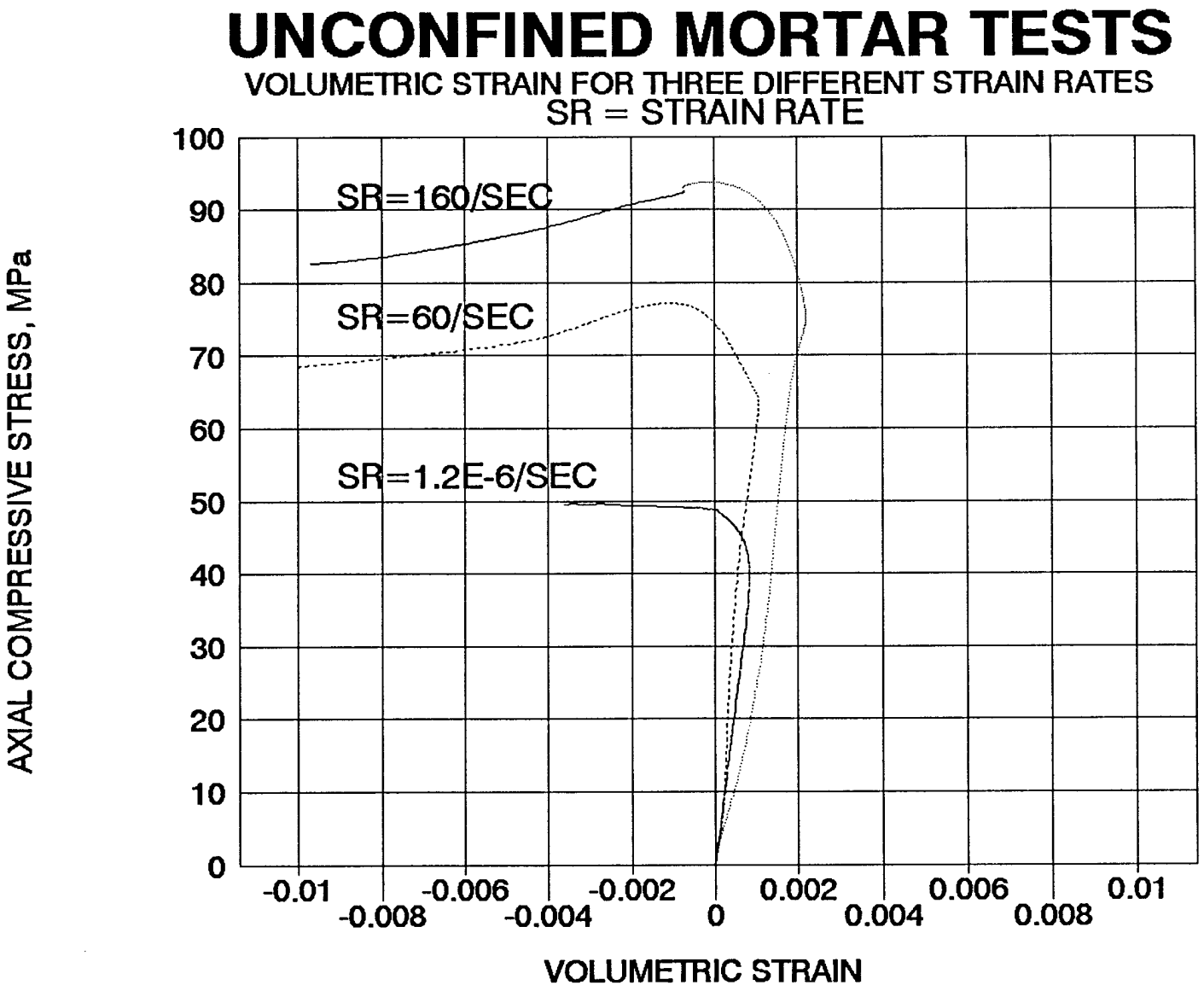

Figure 33. Volumetric strain for three different strain rates versus axial compressive stress for unconfined SHPB test.

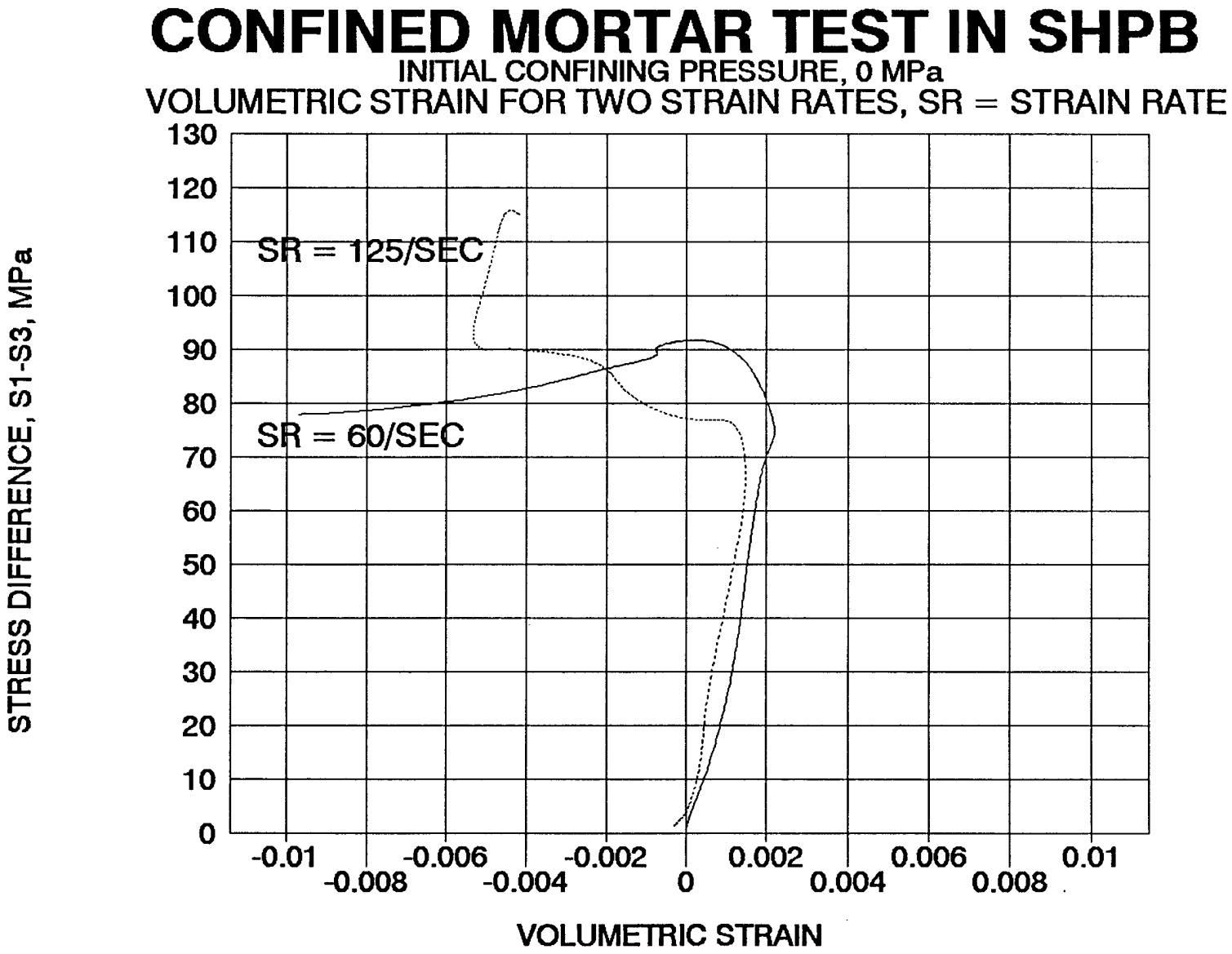

Figure 34. Volumetric strain for two different strain rates versus axial compressive stress for confined SHPB test.

Section IV

A NEW ELASTIC/VISCOPLASTIC CONSTITUTIVE EQUATION FOR MORTAR

1. Introduction

For rock and concrete 3-D dependent constitutive equations have been proposed by one of the co-principal investigators and have extensive exposure in the literature (see for *e.g.* Cristescu et.al. [16, 17, 18]. To calibrate these constitutive equations confined triaxial quasistatic data are necessary. Since for mortar only uniaxial compression quasistatic data were available a simplified elastic/viscoplastic constitutive equation has been developed. It is shown that although simple in concept and in expression the model captures the main features of the material response such as compressibility and dilatancy, strain-hardening, influence of the loading rate, and creep and relaxation. The model can be easily extended to 3-D conditions (see Cristescu [16])).

2. Structure of the Constitutive Equation

We consider that the material response under axisymmetric triaxial conditions can be described as

$$\dot{\varepsilon}_1 = \left(\frac{1}{3G} + \frac{1}{9K}\right)\dot{\sigma}_1 + \left(-\frac{1}{3G} + \frac{2}{9K}\right)\dot{\sigma}_3 + h_1\left\langle f_1(\sigma_1, \sigma_3) - \varepsilon_1\right\rangle, \qquad (4)$$

$$\dot{\varepsilon}_3 = \left(-\frac{1}{6G} + \frac{1}{9K}\right)\dot{\sigma}_1 + \left(\frac{1}{6G} + \frac{2}{9K}\right)\dot{\sigma}_3 + h_3\left\langle f_2(\sigma_1, \sigma_3) - \varepsilon_3\right\rangle \qquad (5)$$

where, $\dot{\varepsilon}_1$ and $\dot{\varepsilon}_3$ are the axial strain rate and transversel strain rate, respectively; σ_1 and σ_3 are the axial and radial stresses, G is the shear modulus, and K is the bulk modulus. In equations (4) and (5) $\langle\ \rangle$ is the Macauley bracket which defines the positive part of any expression,

i.e. $\langle A\rangle=\frac{1}{2}\left(A+|A|\right)$, while h_1 and h_3 are viscosity parameters. It is worthwhile to point out that by introducing a **shearing viscosity** different from the **volumetric viscosity** the particularities of the irreversible volumetric response can be described very accurately. Specifically, it is possible to capture the rate influence on the dilatancy threshold and on the extent of the dilatant zone in the material.

In considering a creep test, assume that at time $t_0=0$: $\varepsilon\left(t_0\right)=0$, $\sigma\left(t_0\right)=\sigma^0$, and for $t\geq t_0$: $\sigma(t)=\sigma(t_0)$. From equations (4) and (5) we get

$$\varepsilon_1(t)=\left[\left(\frac{1}{3G}+\frac{1}{9K}\right)\sigma_1^0+\left(-\frac{1}{3G}+\frac{2}{9K}\right)\sigma_3^0\right]\exp(-h_1 t)+\left[1-\exp(-h_1 t)\right]f_1\left(\sigma_1^0,\sigma_3^0\right)$$

$$\varepsilon_3(t)=\left[\left(\frac{-1}{6G}+\frac{1}{9K}\right)\sigma_1^0+\left(\frac{1}{6G}+\frac{2}{9K}\right)\sigma_3^0\right]\exp(-h_3 t)+\left[1-\exp(-h_3 t)\right]f_1\left(\sigma_1^0,\sigma_3^0\right) \tag{6}$$

Note that when $t\to\infty$, $\varepsilon_1=f_1(\sigma_1,\sigma_3)$ and $\varepsilon_3=f_3(\sigma_1,\sigma_3)$. Thus, the specific expressions of the stabilization boundaries can be determined from quasi-static data. The viscosity parameters can be obtained from compression tests data in SHPB at two different strain rates. Since for mortar only unconfined quasi-static data were available we have fully developed a 1-D stress version of the model. Thus, the stabilization boundaries are considered to be of the form: $\varepsilon_1=F_1(\sigma_1)$ and $\varepsilon_3=F_3(\sigma_1)$. A fourth order polynomial fit the data well, given as

$$F_1\left(a_1,a_2,a_3,a_4,\sigma_1\right)=a_4\sigma_1^4+a_3\sigma_1^3+a_2\sigma_1^2+a_1\sigma_1\,, \tag{7}$$

$$F_3\left(b_1,b_2,b_3,b_4,\sigma_1\right)=b_4\sigma_1^4+b_3\sigma_1^3+b_2\sigma_1^2+b_1\sigma_1 \tag{8}$$

where, $a_1 = 3.522 \cdot 10^{-5}, a_2 = 1.131 \cdot 10^{-6}, a_3 = -6.026 \cdot 10^{-8}, a_4 = 1.06 \cdot 10^{-9}, b_1 = -2.08 \cdot 10^{-6}$, $b_2 = -2.08 \cdot 10^{-6}$, $b_3 = 10^{-7}$, and $b_4 = -1.5 \cdot 10^{-9}$. The dynamic Young modulus E is 28.73 GPa, while the Poisson's ratio ν = 0.2. The viscosity coefficient h_1 can be determined from data obtained in unconfined dynamic tests performed at strain rate $\dot{\varepsilon}^{(1)}$ and $\dot{\varepsilon}^{(2)}$, respectively($\dot{\varepsilon}^{(1)} \neq \dot{\varepsilon}^{(2)}$). Indeed, if $\sigma_1^{(1)}$ and $\sigma_1^{(2)}$ are stresses corresponding to the same value of the axial strain ε_1 and $\dot{\sigma}_1^{(1)}$ and $\dot{\sigma}_1^{(2)}$ the corresponding loading rates, from equation (4) it follows that:

$$h_1 = \frac{\left(\dot{\varepsilon}_1^{(1)} - \dot{\varepsilon}_1^{(2)}\right) - \left(\frac{\dot{\sigma}_1^{(1)} - \dot{\sigma}_1^{(2)}}{E}\right)}{F_1\left(\sigma_1^{(1)}\right) - F_1\left(\sigma_1^{(2)}\right)} \tag{9}$$

If we use data from tests DCMU4 and DCMU5, i.e. $\dot{\varepsilon}^{(1)}$= 60/s, $\dot{\varepsilon}^{(2)}$= 160/s, $\dot{\sigma}_1^{(1)}$= $1.346 \cdot 10^4$ MPa/s, $\dot{\sigma}_1^{(2)} = 2.07 \cdot 10^6$ MPa/s we get $h_1 = 6 \cdot 10^3$ s^{-1}. A formula similar to equation (8) can be used to derive h_3 and for mortar $h_3 = 20 \cdot 10^3$ s^{-1}.

Consider an unconfined compression test at a constant load rate, *i.e.* at time $t_0 = 0$: $\boldsymbol{\varepsilon}(t_0) = \boldsymbol{0}$, $\boldsymbol{\sigma}(t_0) = \boldsymbol{0}$, and for $t \geq t_0$: $\sigma_1(t) = \dot{\sigma}_1^0 t$, $\sigma_3(t) = 0$. Integrating equations (4) and (5) we obtain

$$\varepsilon_1(\sigma_1, \dot{\sigma}_1) = \frac{1}{E}\left(1 - \exp\left[-h_1\left(\frac{\sigma_1}{\dot{\sigma}_1}\right)\right]\right)\frac{\dot{\sigma}_1}{h_1} + \sum_{i=0}^{4}(-1)^i\left(\frac{\dot{\sigma}_1}{h_1}\right)^i\left(F_1^{(i)}(\sigma_1) - F_1^{(i)}(0)\cdot\exp\left[-h_1\left(\frac{\sigma_1}{\dot{\sigma}_1}\right)\right]\right) \tag{10}$$

$$\varepsilon_3(\sigma_1, \dot{\sigma}_1) = \frac{-\nu}{E}\left(1 - \exp\left[-h_3\left(\frac{\sigma_1}{\dot{\sigma}_1}\right)\right]\right)\frac{\dot{\sigma}_1}{h_3} + \sum_{i=0}^{4}(-1)^i\left(\frac{\dot{\sigma}_1}{h_3}\right)^i\left(F_3^{(i)}(\sigma_1) - F_3^{(i)}(0)\cdot\exp\left[-h_3\left(\frac{\sigma_1}{\dot{\sigma}_1}\right)\right]\right) \tag{11}$$

In equations (10) and (11) $F^{(i)}$ stands for the i^{th} derivative of F with respect to σ_1.

If in equations (10) and (11), $\dot{\sigma}_1 \to 0$, we obtain the stabilization boundaries $\varepsilon_1 = F_1(\sigma_1)$ and $\varepsilon_3 = F_3(\sigma_1)$, respectively while for $\dot{\sigma}_1 \to \infty$ we get the corresponding elastic curves. In equations (10) and (11) $F^{(i)}$ stands for the i^{th} derivative of F with respect to σ_1. If in equations (10) and (11), $\dot{\sigma}_1 \to 0$, we obtain the stabilization boundaries $\varepsilon_1 = F_1(\sigma_1)$ and $\varepsilon_3 = F_3(\sigma_1)$, respectively while for $\dot{\sigma}_1 \to \infty$ we get the corresponding elastic curves.

3. Comparison with the data

In the following we present a comparison between the model predictions and unconfined direct compression data in SHPB. The dynamic tests designated as DCMU4 and DCMU5 were done at constant strain rate of 60 /s and 160/s, respectively.

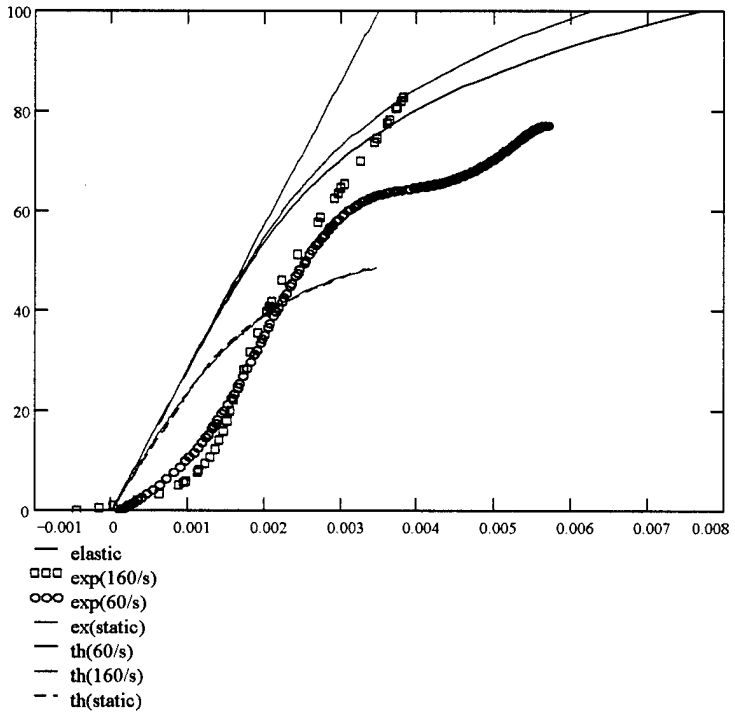

Figure 35. Comparison between the theoretical $\sigma_1 - \varepsilon_1$ curves and data in DCMU4, DCMU5, and quasi-static test.

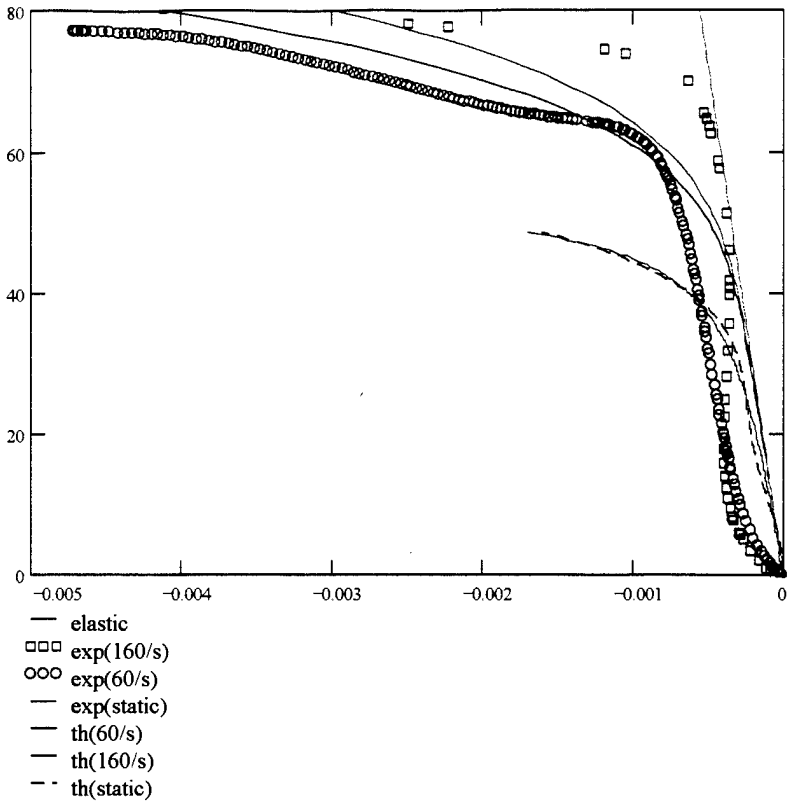

Figure 36. Comparison between the theoretical $\sigma_1 - \varepsilon_3$ curves and data in DCMU4, DCMU5, and quasi-static test

From the axial load (transmitted stress) versus time curve (see Figs 16 and 19) we estimate the average loading rate as $\dot{\sigma}_1^{(1)} = 1.346 \cdot 10^4$ MPa/s, and $\dot{\sigma}_1^{(2)} = 2.07 \cdot 10^6$ MPa/s respectively. Then, using Eqs. (10) and (11) we can plot the theoretical curves $\sigma_1 - \varepsilon_1$ and $\sigma_1 - \varepsilon_3$ corresponding to the constant loading rates $\dot{\sigma}_1^{(1)}$ and $\dot{\sigma}_1^{(2)}$ (see Figures 35 and 36). As expected the static stress-strain curves are less than the dynamic ones. Also, the increase in the strain rate results in a "raising" of all stress-strain curves. The lower parts of the experimental dynamic stress-axial strain curves present upward concavities, which are not due to rate effects but result from other phenomena such as the crushing of asperities at the ends of the specimen. The static stress-strain curves are well reproduced by the model. The theoretical dynamic curves are obtained from the static ones assuming material viscosity and using the concept of overstress. The instantaneous response, i.e. the material response when the strain rate is increased to infinity is modeled as elastic.

It can be noted that the rate influence is correctly described. The theoretical curves correspond to a constant loading rate (the average loading rate in the test) while in tests the loading rate was not constant. Therefore, we cannot expect a perfect agreement between the model and data. However, the general trends of the data are reproduced and for higher values of the stress the comparison is within the natural scatter of the data. Finally the comparison between the model predictions of volumetric strains and data shown in Figure 37 show the ability of the model to reproduce both compressibility and dilatancy.

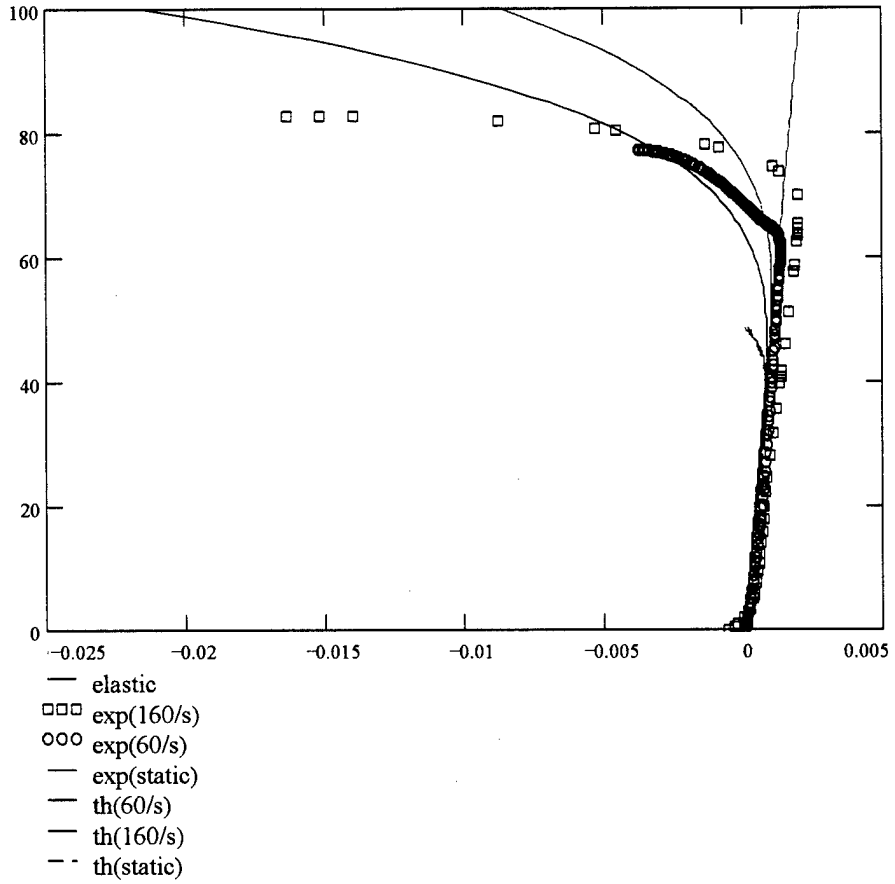

Figure 37. Comparison between the theoretical $\sigma_1 - \varepsilon_V$ curves and data in DCMU4, DCMU5, and quasi-static test

The model developed for 1-D stress conditions could be easily extended to axisymmetric confined conditions. Indeed, it suffices to take the stabilization boundaries of the form

$\varepsilon_1 = F_1\left(a_1'(\sigma_3), a_2'(\sigma_3), a_3'(\sigma_3), a_4'(\sigma_3), \sigma_1 \right)$ and $\varepsilon_3 = F_3\left(b_1'(\sigma_3), b_2'(\sigma_3), b_3'(\sigma_3), b_4'(\sigma_3), \sigma_1\right)$ such that $a_i'(0) = a_i$ and $b_i'(0) = b_i$, $i = 1...4$, the specific expressions of the functions a_i' and b_i' being determined from quasi-static confined data. Since for confined triaxial conditions,

$$\varepsilon_1 = \varepsilon + \bar{\varepsilon}, \varepsilon_3 = \varepsilon - \frac{\bar{\varepsilon}}{2} \tag{12}$$

$$\sigma_1 = \sigma + \frac{2}{3}\bar{\sigma}, \sigma_3 = \sigma - \frac{1}{3}\bar{\sigma} \tag{13}$$

the model Eqs. (4) and (5) can be written in terms of the stress invariants $\sigma = \frac{tr\,\sigma}{3}$, $\bar{\sigma} = \sqrt{\frac{3}{2} tr(\sigma')^2}$ and the strain invariants $\varepsilon = \frac{tr\,\varepsilon}{3}$, $\bar{\varepsilon} = \sqrt{\frac{2}{3} tr(\varepsilon')^2}$ as

$$\dot{\varepsilon} = \dot{\varepsilon}^E + \dot{\varepsilon}^I \tag{14}$$

$$\dot{\varepsilon}^E = \frac{\dot{\sigma}}{2G} + \left(\frac{1}{3K} - \frac{1}{2G}\right)\dot{\sigma}\, \boldsymbol{1} \tag{15}$$

$$\dot{\varepsilon}^I = A\left(\sigma, \bar{\sigma}, \varepsilon, \bar{\varepsilon}\right)\frac{\sigma'}{\bar{\sigma}} + B\left(\sigma, \bar{\sigma}, \varepsilon, \bar{\varepsilon}\right)\boldsymbol{1} \tag{16}$$

where, $\dot{\varepsilon}^E$ denotes the elastic strain rate , $\dot{\varepsilon}^I$ the irreversible (viscoplastic) strain rate, "tr" stands for the trace operator, σ is the Cauchy stress tensor, σ' the stress deviator, and $\boldsymbol{1}$ the second order identity tensor.

4. Conclusions

A rate dependent constitutive model for mortar has been developed. The model reproduces

- strain-hardening,
- influence of the loading rate,
- creep and relaxation,

- observed compressibility and dilatancy.

The model can be easily generalized to 3-D conditions.

Section V

CONCLUSION AND RECOMMENDATIONS

Using strain gages mounted on test specimens one is able to follow changes in compressibility and dilatancy in unconfined and confined quasistatic and dynamic mortar tests. The split Hopkinson pressure bar (SHPB) proved to be a useful tool in determining dynamic dilantacy in mortar compression under light confinement and dynamic shear response of mortar. A new elastic/viscoplastic constitutive equation was developed for mortar and was shown to reproduce strain-hardening, load note effects, creep and relaxation, observed compressibility and dilantacy.

Continued testing at higher confining pressure is required to produce essential parameters in further development of the elastic/viscoplastic constitutive equation to include effects of confinement. Additional testing in concrete and granite are required to characterize these materials for viscoplastic response.

Section VI

REFERENCES

1. Department of the Army, Navy and Air Force, Washington. *Structures to resist the effects of accidental explosions,* June 1969.

2. Houze, F. E. An overview of projectile penetration into geological materials, with emphasis on rocks. *International Journal of Rock Mechanics Mining Sciences & Geomechanics Abstracts, 27(1):1~14,* 1990.

3. Ross, C. A., Kuennen, S. T., and Tedesco, J. W. Experimental and numerical analysis of high strain-rate concrete tensile tests. In Shah, S. P., Swartz, S. E., and Wang, M. L., editors, *Micromechanics of Failure of Quasi-Brittle Materials,* pages 353-364. Elseveir Applied Science, London, 1990.

4. Malvern, L. E., Jenkins, D. A., and Ross, C. A. Dynamic compressive testing of concrete. In *Proceedings of Second Symposium on the Interaction of Non-Nuclear Munitions with Structures,* pages 194-199, Panama City Beach, FL, April 1985.

5. Murtha, R. and Crawford, J. Dynamic shear failure predictions of shallow-burried reinforced-concrete slabs. Technical Report M-51-81-04, Civil Engineering Laboratory, Port Huencme, CA, May 1981.

6. Young, L. A., Streit, B. K., Peterson, K. J., Read, D. L., and Maestas, F. A. Effectiveness/vulnerability assessments in three dimensions (eva-3d) versions 4.1f and 4.1c users manual – revision a. Technical Report WL-TR-96-7000, Air Force Wright Laboratory Armament Directorate, November 1995.

7. Richard, H. A. A new compact shear specimen. *International Journal of Fracture,* 17:105-107, 1981.

8. Ross, C. A. Split-Hopkinson pressure bar tests. Technical Report ESL-TR-88-82, Air Force Engineering and Services Center, March 1989.

9. Bazant, Z. P. and Pfeiffer, P. A. Tests of shear fracture and strain-softening in concrete. In *Proceedings of the Second Symposium on the Interaction of Non-nuclear Munitions with Structures,* pages 254-264, Panama City Beach, FL, 1985.

10. Iosipescu, N. New accurate procedure for single shear testing of metals. *Journal of Materials*, 2(3):537-566, September 1967.

11. Barr, B. The fracture characteristics of FRC materials in shear. In Shah, S. P. and Batson, G. B., editors, *Fiber Reinforced Concrete Properties and Applications,* number SP-105, pages 27-53. American Concrete Institute, Detroit, 1987.

12. Barr, B. Compact shear test specimens for FRC materials. *Composites,* 18(1):54-60, January 1987.

13. ADINA, "A Finite Element Computer Program for Automatic Dynamic Incremental Nonlinear Analysis Reports ARD 87-1 ADINA R&D, Watertown, MA, 1987.

14. Follansbee, P. S. The Hopkinson bar. In *Metals Handbook,* volume 8, Mechanical Testing, pages 198-203. American Society for Metals, 9 edition, 1989.

15. Malvern, L. E. and Jenkins, D. A., Dynamic Testing of Laterally Confined Concrete. Tech. Report ESL-TR-89-47. AF Engineering and Services Center, September 1990.

16. Cristescu, N., "Rock Dilatancy in Uniaxial Tests", *Rock Mechanics*, **15**, 1982, pp. 133-144.

17. Cristescu, N. D., Rock Rheology, Kluwer Academic Publishers, Dordrecht, 1989.

18. Cristescu, N. D. and Hunsche, U., Time Effects in Rock Mechanics, John Wiley & Sons, Chichester, 1998.